

## Article

# A Computer Tool for Modelling CO<sub>2</sub> Emissions in Driving Cycles for Spark Ignition Engines Powered by Biofuels

Karol Tucki 

Department of Production Engineering, Institute of Mechanical Engineering, Warsaw University of Life Sciences, Nowoursynowska Street 164, 02-787 Warsaw, Poland; karol\_tucki@sggw.edu.pl; Tel.: +48-593-45-78

**Abstract:** A driving cycle is a record intended to reflect the regular use of a given type of vehicle, presented as a speed profile recorded over a certain period of time. It is used for the assessment of engine pollutant emissions, fuel consumption analysis and environmental certification procedures. Different driving cycles are used, depending on the region of the world. In addition, drive cycles are used by car manufacturers to optimize vehicle drivelines. The basis of the work presented in the manuscript was a developed computer tool using tests on the Toyota Camry LE 2018 chassis dynamometer, the results of the optimization process of neural network structures and the properties of fuels and biofuels. As a result of the work of the computer tool, the consumption of petrol 95, ethanol, methanol, DME, CNG, LPG and CO<sub>2</sub> emissions for the vehicle in question were analyzed in the following driving tests: Environmental Protection Agency (EPA US06 and EPA US03); Supplemental Federal Test Procedure (SFTP); Highway Fuel Economy Driving Schedule (HWFET); Federal Test Procedure (FTP-75-EPA); New European Driving Cycle (NEDC); Random Cycle Low (×05); Random Cycle High (×95); Mobile Air Conditioning Test Procedure (MAC TP); Common Artemis Driving Cycles (CADC-Artemis); Worldwide Harmonized Light-Duty Vehicle Test Procedure (WLTP).



**Citation:** Tucki, K. A Computer Tool for Modelling CO<sub>2</sub> Emissions in Driving Cycles for Spark Ignition Engines Powered by Biofuels. *Energies* **2021**, *14*, 1400. <https://doi.org/10.3390/en14051400>

Academic Editor: Constantine D. Rakopoulos

Received: 9 February 2021  
Accepted: 1 March 2021  
Published: 4 March 2021

**Publisher's Note:** MDPI stays neutral with regard to jurisdictional claims in published maps and institutional affiliations.



**Copyright:** © 2021 by the author. Licensee MDPI, Basel, Switzerland. This article is an open access article distributed under the terms and conditions of the Creative Commons Attribution (CC BY) license (<https://creativecommons.org/licenses/by/4.0/>).

**Keywords:** car; fuel; biofuel; neural model

## 1. Introduction

The dynamic development of technology, which the automotive industry has seen for many years, includes both achieving an appropriate level of vehicle performance and meeting appropriate environmental protection requirements [1–4]. Keeping exhaust gas emissions under the permissible limits is the basic criterion that determines the directions of further development of engines used to drive motor vehicles [5–8]. Increasingly restrictive legal regulations are introduced to protect the climate [9–12]. The European Union (EU) has long been setting ambitious climate goals, which will not be achievable without reducing greenhouse gas emissions in transport—which consumes a third of the energy in the EU [13–15]. It is the transport sector in the EU that accounts for almost 30% of total CO<sub>2</sub> emissions, 72% of which comes from road transport [16,17]. Passenger cars are responsible for 60.7% of all CO<sub>2</sub> emissions from road transport in Europe [18,19].

Additionally, in the United States, car exhaust gases are the main source of greenhouse gas emissions, thus causing climate change [20–22]. The local permissible exhaust emission standards are based on research by a federal US body—the Environmental Protection Agency (EPA) [23,24]. Greenhouse gas emissions from transport account for approximately 28 percent of total US greenhouse gas emissions [25,26].

In China, combustion tests are a mixture of the abovementioned European and American regulations [27,28]. Work is also underway on a new type of test, which will be even more complicated and will much better reflect actual conditions [29,30]. The Chinese transport sector is responsible for around 12% of domestic emissions [31–34].

Each new passenger car must meet exhaust gas toxicity standards before it is introduced to the market [35–37]. The test conditions depend on the vehicle class and the

country of destination [38–40]. Such tests, carried out in laboratory conditions, enable the repeatability and comparability of the obtained results [41–43]. By carrying out such tests, it is possible to avoid many of the risk factors associated with the actual road testing of vehicles that will affect fuel consumption—such as driving style, terrain or weather conditions. In order to execute these tests, a chassis dynamometer is needed (on a roller dynamometric stand) with adjustable motion resistance and execution of driving cycles [44–46].

Until August 2017, light vehicles in the European Union (with a reference mass not exceeding 2610 kg) were tested with the standard New European Driving Cycle (NEDC) driving test that included four repeated Urban Driving Cycles (UDCs) and one Extra Urban Driving Cycle (EUDC) [47–50]. Since September 2017, there has been a new procedure in force in the EU in the area of fuel consumption, carbon dioxide and exhaust emission standards: the Worldwide Harmonized Light-Duty Vehicles Test Procedure (WLTP) EU [51–53]. Although the WLTP is also a test carried out under laboratory conditions, it covers situations possibly closest to everyday actual operating conditions. Four speed ranges are measured from the moment the engine is started: up to 60, up to 80, up to 100 and over 130 km/h. During each of these phases, the vehicle always slows down and accelerates [54,55]. The maximum speed is 10 km/h more than that of the NEDC test. The average speed is 47 km/h—much higher than the previous 33 km/h. A complete WLTP cycle takes about 30 min, whereas the NEDC only takes about 20 min [56–58]. The cycle distance has more than doubled and is now 23 km instead of the previous 11 km. Unlike the NEDC cycle, the requirements of the car's electrical system and additional equipment are also taken into account: its weight, aerodynamics and rolling resistance [59,60]. Any additional vehicle equipment that is highly energy-consuming, such as those with air conditioning or heated seats, remains excluded from the WLTP test [61,62].

The conditions for dynamometric testing and vehicle loading are based on the strict guidelines of the WLTP test procedure including several Worldwide Harmonized Light-Duty Vehicles Test Cycles (WLTC) [63,64]. These cycles are applicable to vehicle categories with different power-to-weight ratios (unladen weight) [65,66].

In addition to the WLTP, the EU Commission also enforces the so-called Real Driving Emissions (RDE) as an additional approval requirement under Article EU6d of the directive for emissions [67–70]. Contrary to the NEDC and WLTP, the RDE tests set out acceptable limits for nitrogen oxides (NO<sub>x</sub>) and solid particle emissions in real conditions [71,72]. The RDE does not require a strictly defined driving cycle. Its parameters, including distance, acceleration, outside temperature, wind strength or traffic intensity, are freely selected within the specified statistical boundary conditions [73–75].

The European project Assessment and Reliability of Transport Emission Models and Inventory Systems (ARTEMIS) developed a chassis dynamometer procedure called Common Artemis Driving Cycles (CADC) that can be characterized by stronger acceleration, higher driving dynamics and a realistic proportion of high speeds (with peaks up to 130 and 150 km/h) [76–78]. The cycles realized as part of the procedure include three driving plans: urban (distance 4.8 km), rural road (distance 17.2 km) and two variants of the motorway plan (distances of 28.7 and 29.5 km) [79–81].

There is a test procedure in the EU for measuring additional fuel consumption and pollutant emissions caused by the operation of the Mobile Air Conditioning (MAC) system in a passenger car [82–84]. The procedure for a physical test of the whole vehicle on a chassis dynamometer includes a double test run (with MAC ON and MAC OFF) with the same three phases of the fixed condition of the test cycle [85,86].

In the United States of America, the Federal Transient Procedure (FTP-75) test is used to evaluate the environmental performance of passenger cars and delivery vans, whereas the Highway Federal Extra Test (HWFET) test is used to assess fuel consumption [87–90]. The FTP-75 simulates a city route with frequent stops, combined with both a cold and hot start transition phase [91–93]. The entire cycle, in which the vehicle travels 17.77 km, at an average speed of 34.12 km/h, takes about 31 min [94,95]. Cycle FTP-75 is among two variants of the Urban Dynamometer Driving Schedule (UDDS).

Furthermore, the Supplemental Federal Test Procedure (SFTP) applies [96,97]. It was developed for the purposes of a driving analysis of a vehicle with an air conditioner, dynamic changes in its driving speed as well as acceleration and deceleration of the vehicle. The high speed and rapid acceleration analysis was covered by the US06 SFTP cycle and standards [98–101]. During the cycle, the car covers a distance of 12.8 km in 596 s, reaching a maximum speed of 129.2 km/h [102,103]. An additional SC03 SFTP test procedure covers an analysis of emissions related to the use of air conditioners on vehicles certified under the FTP-75 test cycle [104–106]. In this test, the vehicle travels 5.8 km in 596 s, reaching a maximum speed of 88.2 km/h [107,108]. It should be emphasized that the SFTP emission levels are a combination of the emission levels of the two test cycles and the FTP cycle. This means that the SFTP emissions from each test group of vehicles must meet all SFTP and FTP emission standards [109]. In addition, there is the California Unified Cycle LA92 [110].

The diminishing resources of natural fossil fuels and the growing demand for energy pose serious social, technological and scientific challenges [111–115]. Alternative fuels have been developed for many years, and their use in the automotive industry will undoubtedly continue to be verified in the context of road tests [116–120]. Alternative fuels for internal combustion engines are defined in relation to the classic liquid petroleum fuels, such as petrol for spark ignition engines and diesel oil for compression ignition engines [121–123]. All other fuels for internal combustion engines are an alternative to classical liquid petroleum fuels [124–126].

Among the methods of fuel classification may be their state of matter [127–130]. In the case of engines, liquid and gaseous fuels seem predominant, and the only example of solid fuel in the literature is coal dust [131,132]. Further non-renewable alternative liquid fuels include fossil coal processing products and non-petroleum mineral oil processing products [133–137]. The properties of respective fuels depend on their chemical composition [138–140].

The most popular of the fuels produced from crude oil is petrol [141,142]. The refining process begins with distillation. The individual distillation fractions are processed in order to obtain base substances that can later be used in fuels and lubricants [143,144]. The physical properties of petrol have a great influence on the entire fuel supply system and combustion process [145–147]. Therefore, petrol must meet a number of requirements regarding its volatility, octane number and the propensity to form engine deposits. Petrol is made up of a mixture of alkanes and cycloalkanes. The calorific value of petrol, depending on the exact composition of the fuel, is 45.8 MJ/kg. The average consumption of 1 L of petrol per 100 km corresponds to approximately 2.39 kg CO<sub>2</sub>/km [148,149]. The volatility of petrol is always included in the specifications (e.g., EN 228 in Europe and ASTM D 4814 in the USA). In Europe, conventional unleaded petrol must have a density between 0.725 and 0.78 g/cm<sup>3</sup>, in the USA from 0.745 to 0.765 g/cm<sup>3</sup> [150,151].

Non-renewable alternative gaseous fuels mainly include fuels based on petroleum gas (consisting mainly of propane and butane)—Liquefied Petroleum Gas (LPG)—fuels based on natural gas whose main component is methane—Compressed Natural Gas (CNG), Liquefied Natural Gas (LNG) as well as fossil coal processing products [152–156].

LPG is a by-product of natural gas production processes or crude oil distillation processes in refineries. Depending on the region of the world, its composition includes 90% propane, 2.5% butane, traces of ethane and propylene with heavy hydrocarbons. LPG as a fuel for transport is a source of cleaner energy, since it emits about 20% less carbon compounds than petrol. The reduction in pollutants in transport thanks to LPG can amount to approx. 10–15% less CO<sub>2</sub>, 20% less CO and 60% less hydrocarbons [157–159].

CNG is a natural gas compressed to 20–25 MPa, used in spark ignition and compression ignition engines. Under normal conditions, the energy value of 1 m<sup>3</sup> of CNG is approximately equal to the energy value of 1 L of petrol. The mass of 1 m<sup>3</sup> of natural gas under normal conditions is approximately 0.7 kg and depends on the gas composition. The main component of CNG is methane [160,161].

The most important renewable liquid fuels are Pure Vegetable Oils (PVO), esters of higher carboxylic acids: methyl Fatty Acid Methyl Esters (FAME), ethyl Fatty Acid Ethyl

Esters (FAEE) and alcohols, mainly primary: methanol and ethanol; secondary, alcohol derivatives (mainly ethers); and liquid products of biomass processing Biomass to Liquid (BTL) [162–164].

Among the abovementioned renewable liquid fuels, ethanol and methanol warrant special attention.

Ethanol is obtained from plant products through the process of the fermentation of sugar. The largest disadvantage of ethanol is its low calorific value (30.4 kJ/g). In relation to a liter, this value is 1/3 lower than for petrol, i.e., 10 L of petrol corresponds to approx. 15 L of ethanol (the calorific value of petrol is 45.0 kJ/g). The octane number of this fuel can exceed 108. This enables an increase in the compression ratio or the boost pressure. Commercially, ethanol fuels are sold with the E prefix (e.g., E85 contains 85% ethanol and 15% petrol) [165–167].

Methanol is a technical alcohol that is obtained by the dry distillation of wood or evaporation of coal. Its properties are similar to ethanol, but it has a lower calorific value (20.1 kJ/g). The octane number of methyl alcohol exceeds even 110. A large part of its mass is occupied by oxygen, one atom of which is present in each methanol molecule. This means that its calorific value is much lower than that of petrol or ethanol. Methanol is also used to power speedway motorcycles equipped with engines with compression ratios exceeding 16 [168–172].

For many years, efforts have been made to develop dedicated tools for computer simulations of the analysis of the amount of pollutants emitted from motor vehicles.

An example of such a tool is the Vehicle Energy Consumption Calculation Tool (VECTO) [173–175]. The simulation tool launched by the European Commission is used to calculate the amount of fuel consumed and carbon dioxide emitted by brand new trucks. The tool calculates driving behavior, load capacity, vehicle configurations, axle configurations, vehicle weight, engine characteristics (engine capacity, fuel map and full load curve), aerodynamic drag and tire rolling resistance. The VECTO calculates the fuel consumption in liters per 100 km and the fuel consumption per ton-kilometer transported, as well as the CO<sub>2</sub> emissions. The program can affect the fuel efficiency of the fleet, due to its thorough analysis of fuel consumption in various vehicle configurations [176–179].

Another tool used as a fuel consumption simulator for passenger cars and delivery vans was CO<sub>2</sub>Mpas. It enabled a simulation run that showed the results that a given vehicle with WLTP tests would achieve in the NEDC test. The tool used correlation methods [180–182].

The literature describes tools for the analysis of pollutant emissions from bus fleets in urban areas [183]. The proposed solution uses the results of measurements made with on-board instrumentation and the calculation method to estimate the emissions and fuel consumption as a function of vehicle parameters and the operating cycle.

The aim of this work was to build a computer tool for simulating driving tests as a function of the consumption of selected fuels and biofuels and CO<sub>2</sub> emissivity. The developed tool is dedicated to vehicles with a spark ignition engine.

## 2. Materials and Methods

The list below contains a set of the most important quantities used in the calculations with the appropriate symbols and units (Table 1).

The development of the simulation model for driving tests was based on the research of the Toyota Camry LE 2018 and published [184]. Table 2 below presents the most important technical parameters of the vehicle and the factors necessary to be used in driving tests and programs generating the required waveforms: vehicle speed, gear number, clutch engagement and pedal position. The values of the Ratio  $n/v$  coefficient for individual runs were calculated on the basis of the dependencies, including the data contained in [185]:

$$\text{Ratio } n/v = n_{\text{engine}} / v_{\text{vehicle}} \text{ [h/(km}\cdot\text{min)]} \quad (1)$$

**Table 1.** Abbreviations, symbols and units used in the paper.

Parameter	Description	Unit
$n_{\text{engine}}$	Engine rotational speed for the given gear number	$\text{min}^{-1}$
$v_{\text{vehicle}}$	Vehicle speed for the given gear number	km/h
$x_i$	Input signals for the neuron	
$w_i, v_i$	Weight values of neurons in individual layers	
$b_i$	Polarity values of neurons in individual layers	
$y_i$	Given learning values	
$d_i$	Values of network responses in the learning process	
$\text{Fuel}_i$ real cycle	Mass of fuel consumed in the <i>i</i> th real road test carried out by EPA (tests: US 06, US highway, FTP-75)	kg
$\text{Fuel}_i$ simul cycle	Mass of fuel consumed in the <i>i</i> th road test from the developed simulation (tests: US 06, US highway, FTP-75)	kg
$n_{\text{engine}}$	Measured value of the engine rotational speed	$\text{min}^{-1}$
$d\text{Fuel}_{\text{Perto195}}$	Instantaneous values of the fuel stream for petrol 95	kg/s
$T_{\text{engine}}$	The torque produced by the motor	N·m
$\text{Cal}_i$	Calorific value for <i>i</i> fuel	J/kg
$w_i$	Mass fraction of <i>i</i> th fuel in the mixture	kg/kg
$\text{Cal}_{\text{Petrol95}}$	Calorific value for petrol 95	J/kg
$\text{Cal}$	Calorific value for other fuel	J/kg
$C_i$	Mass fraction of carbon in <i>i</i> th fuel	kg/kg
$w_i$	Mass fraction of <i>i</i> th fuel in the mixture	kg/kg

**Table 2.** Parameters of the vehicle used in the research for driving tests [185,186].

Parameter	Description	Unit
Vehicle (MY, Make, Model)	2018 Toyota Camry LE	-
Equivalent test mass	1644	kg
Rated power (declared)	151	kW
Rated engine speed (declared)	7000	$\text{min}^{-1}$
Idling engine speed (declared)	800	$\text{min}^{-1}$
Max vehicle speed(declared)	240	km/h
Number of gears	8	-
Ratio $n/v_1$ , gear 1	120.93	h/(km·min)
Ratio $n/v_2$ , gear 2	69.75	h/(km·min)
Ratio $n/v_3$ , gear 3	44.92	h/(km·min)
Ratio $n/v_4$ , gear 4	33.54	h/(km·min)
Ratio $n/v_5$ , gear 5	28.10	h/(km·min)
Ratio $n/v_6$ , gear 6	23.04	h/(km·min)
Ratio $n/v_7$ , gear 7	18.61	h/(km·min)
Ratio $n/v_8$ , gear 8	15.50	h/(km·min)
Target Coeff $f_0$	113.82	N
Target Coeff $f_1$	0.5442	N/(km/h)
Target Coeff $f_2$	0.02811	N/(km/h) <sup>2</sup>

### 2.1. Building a Quantitative Model

In order to construct a quantitative model that would enable the calculation of the instantaneous value of the fuel flow as a function of engine speed, engine torque, transmission gear number and vehicle speed, published data were used, which were obtained during Toyota Camry LE 2018 tests on a chassis dynamometer [184].

Figure 1 presents the set of points obtained during vehicle tests on a chassis dynamometer, converted to the value of hourly fuel consumption as a function of engine speed and torque generated by the engine.

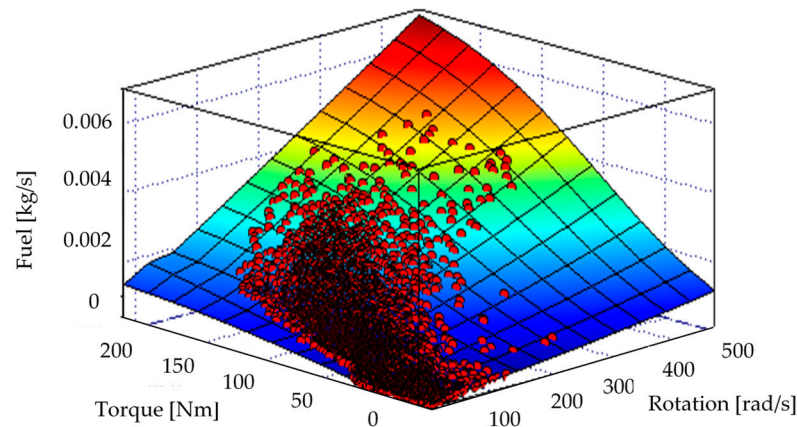


**Figure 1.** Measurement points of hourly fuel consumption as a function of engine rotational speed and engine torque, used to build the quantitative model [184].

The EPA published data included measurement points from actual measurements of the vehicle under consideration on a chassis dynamometer for 6 road tests (UDDS, HWFET, US06, LA92, WLTC and NEDC), for which multiple test repetitions were also provided. These data in spreadsheet form contained instantaneous values of engine speed, engine load torque, vehicle speed, transmission gear number, fuel consumption, etc. These were recorded during the EPA's surveys every 0.1 s. A total of about 350,000 measurement points were used to build the neural model and verify its performance. To build the neural model, about 80% of the available data were used as a learning set, while about 20% of the data were used in the process of verifying the performance of the developed simulation.

In order to construct a quantitative model of instantaneous fuel consumption as a function of engine rotational speed and its generated torque, structures of the "Multilayer Feedforward Backpropagation Network" neural networks with approximating properties were used. The neural network structure itself used (in the hidden layers) a non-linear  $F_1(x)$  activating function determined by the dependency, and a linear  $F_2(x)$  activating function (in the output layer), in the following form:

$$F_1(x) = \frac{2}{1 + \exp(-2 \sum_{i=1}^n w_i x_i + b_i)} \quad (2)$$

$$F_2(x) = \sum_{i=1}^n v_i x_i + b_i \quad (3)$$

In the learning process of the network, the Levenberg–Marquardt algorithm was used, the basis of which is the optimization process through finding the minimum value of the objective function defined as the average value of the sum of squared differences between the current values of the network outputs and the assigned values, in the following form:

$$\Delta \bar{e}^2 = \frac{1}{m} \sum_{i=1}^m (d_i - y_i)^2 \quad (4)$$

Figure 2 below shows a general scheme of the neural network structure that complies with the abovementioned relationships. The "Neural Network Module Version 3.0" library was applied within the Scilab 6.1.0 [187,188] numerical software environment in order to build the neural model.

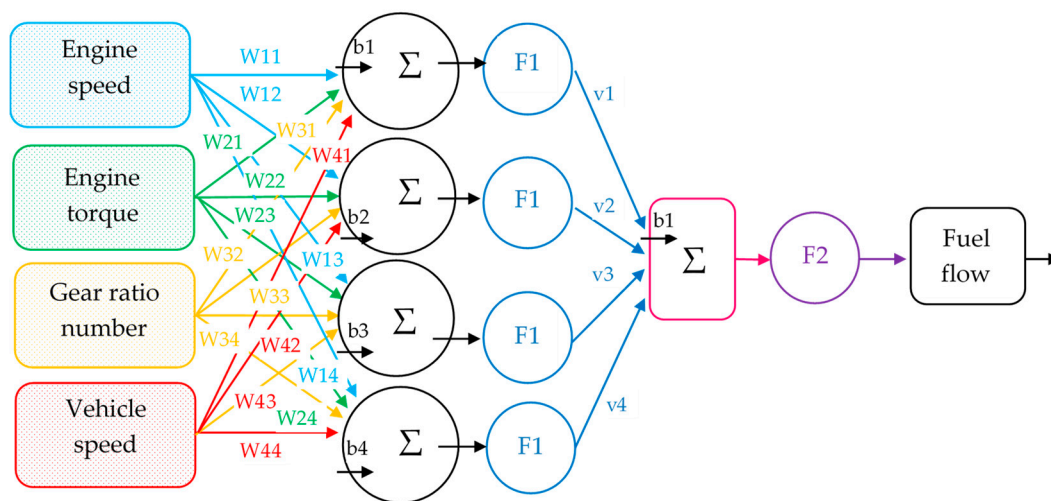


Figure 2. A general scheme of the structure of the neural network applied [187,188].

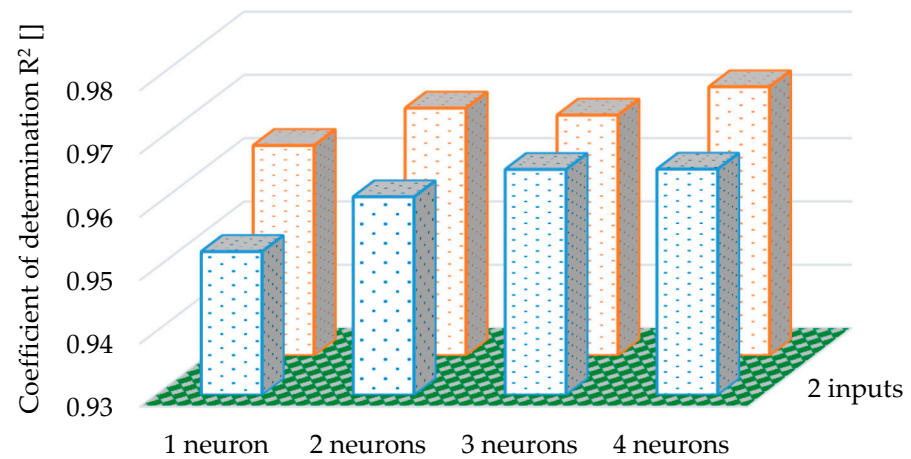
In order to obtain a neural model with the highest possible extent of adjustment to the research data published by EPA [184], an optimization process of the selection of the neural network structure was carried out, which included the change in the number of input parameters, engine rotational speed, engine torque, vehicle gear number, vehicle speed and the change in the number of hidden neurons. In the optimization process, a scalar objective function was used, according to the following dependence:

$$\text{minimum} \left( \frac{\sum_{i=1}^n |\text{Fuel}_i \text{ real cycle} - \text{Fuel}_i \text{ simul cycle}|}{\sum_{i=1}^n \text{Fuel}_i \text{ real cycle}} \right) [\text{kg}] \quad (5)$$

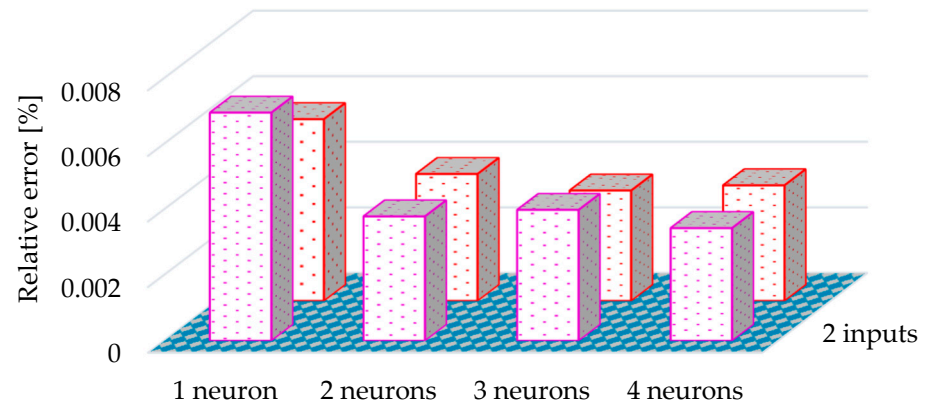
Figure 3 presents selected results of the optimization process for different network structures in question, which differ in the number of input parameters and the number of neurons in the hidden layer, which, in many iterations, obtained the greatest degree of adjustment to the research data.

For the subsequent stages of building a vehicle simulation in road tests, a neural network structure was selected with two inputs for the input signals, engine rotational speed and engine torque, as well as three neurons in the hidden layer.

The selected neural network structure, which was characterized by achieving the smallest relative error value during the learning process for the learning data set, was verified using verification data, which represented approximately 20% of the actual vehicle test data on the chassis dynamometer for the considered tests published by the EPA. Again, the relative error between the simulation fuel consumption result and the real-world test fuel consumption, calculated from Equation (5), did not exceed 0.4%.



(a)



(b)

**Figure 3.** Summary of learning results for the best-adjusted neural networks for the characteristic of specific hourly fuel consumption. The calculated determination coefficient  $R^2$  and the relative error between the model and actual data; 1st and 2nd inputs: engine rotational speed and engine torque; 3rd input: vehicle gear number; 4th input: vehicle speed: (a) coefficient of determination  $R^2$  [-]; (b) relative error [%].

## 2.2. Theoretical Assumptions of the Driving Test Simulator

The published test results on the chassis dynamometer were obtained with the use of standard commercial 95 octane petrol fuel. The presumptions of the work conducted on the vehicle simulation in driving tests were to introduce a functionality that would enable the definition of the consumption of other fuels used to power spark ignition engines. With the use of the neural model ( $f_{Net}$ ), on the basis of the instantaneous values of the torque generated by the engine ( $T_{engine}$ ) and the engine speed ( $n_{engine}$ ), the instantaneous values of the fuel flow for petrol 95 are obtained from the following dependence:

$$\frac{dFuel_{Petrol95}}{dt} = f_{Net}(n_{engine}, T_{engine}) [kg/s] \quad (6)$$



Then, the simulation calculates the calorific value, in the case of using a fuel other than petrol 95 or fuel mixtures from the relationship:

$$\text{Cal} = \sum_{i=1}^n w_i \cdot \text{Cal}_i \text{ [J/kg]} \quad (7)$$

It was assumed in the calculations that, for the instantaneous load value arising from the rotational engine speed and the engine-generated torque, a stream of another fuel must provide the same amount of energy over time as in the case of petrol 95. The efficiency of operation in the case of an engine powered by other fuels remains the same as for petrol 95, for each given calculation point. In this case, the instantaneous stream of fuels other than petrol 95 is calculated from the following dependence:

$$\frac{d\text{Fuel}}{dt} = \frac{d\text{Fuel}_{\text{Petrol95}}}{dt} \frac{\text{Cal}_{\text{Petrol95}}}{\text{Cal}} \text{ [kg/s]} \quad (8)$$

Table 3 presents the basic parameters of the fuels used in the simulation:

**Table 3.** Basic parameters of the fuels used in the simulation [189–193].

Parameter	Petrol 95	Ethanol	Methanol	DME	CNG	LPG
Calorific [MJ/kg]	43.5	26.7	19.93	28.4	50.0	46.3
Carbon [%]	86.4	52.1	37.5	52.1	74.9	81.7
Hydrogen [%]	13.6	13.1	12.6	13.1	25.1	18.3
Oxygen [%]	0.0	34.7	49.9	34.7	0.0	0.0

The presented properties of CNG fuel refer to the mixture which is used to power vehicles in a compressed form to the value of about 20MPa, containing 96–98% of methane with a minimum amount of other polluting gases and water vapor.

Figure 4 shows the waveforms of the instantaneous value of the specific fuel consumption as a function of the engine rotational speed and the engine-generated torque for 6 types of fuels used in the simulation (petrol 95, ethanol, methanol, DME, CNG and LPG).

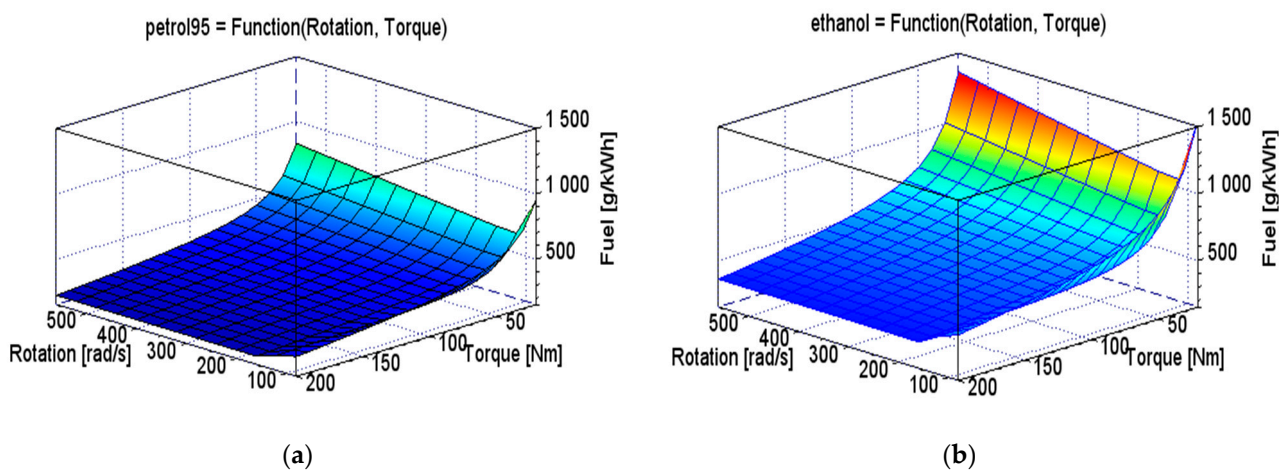


**Figure 4.** Cont.

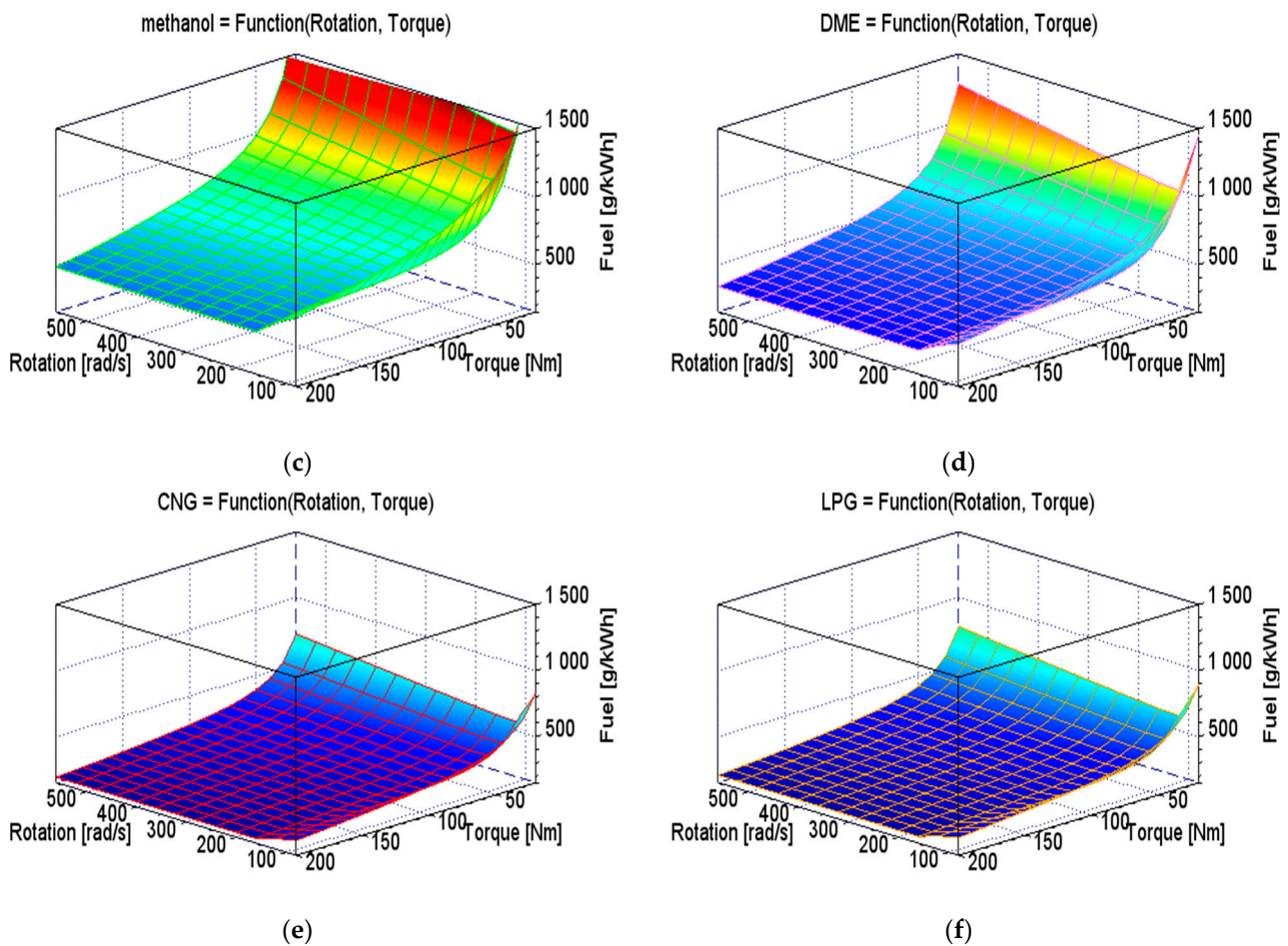


**Figure 4.** A model of individual fuel consumption characteristics built with the use of a neural network and used in further simulations: (a) petrol 95; (b) ethanol; (c) methanol; (d) DME; (e) CNG; (f) LPG.

In order to calculate the CO<sub>2</sub> emissivity, the mass content of carbon in the analyzed fuel was calculated. This was performed on the basis of the available information on the chemical compositions of the individual mixture components, the mass content of the fuel in the mixture and the instantaneous fuel stream that resulted from the conditions of the engine operation conditions using the following relationship:

$$\frac{dCO_2}{dt} = 3.664 \cdot \frac{dFuel}{dt} \cdot \sum_{i=1}^n w_i \cdot C_i \quad [kg/s] \quad (9)$$

### 2.3. Driving Test Generator

The most labor intensive process was teaching neural network structures. In this study, in order to obtain an optimal neural model for determining the instantaneous value of fuel consumption as a function of the engine speed and torque, structures with 2 and 3 inputs and a variable number of neurons in the hidden layer (1–4) were used. The structure learning process for fixed inputs and number of neurons in the hidden layer were repeated at least 100 times with a fixed minimum number of learning epochs of 1000. In total, the process of learning neural network structures to select the most fitting model took about 13 h. However, the process of simulation by the selected neural model of selected driving tests took about several minutes. In the developed simulation, no correlation was made between the simulation time and the actual duration of the driving test.

Based on the collected data of operational parameters of the vehicle in question and using the “Gearshift calculation tool” [194,195] application, runs for simulation control were created for the following drive tests:

- US 06—The US06 (SFTP) [196,197];
- US highway—Highway Fuel Economy Driving Schedule (HWFET) [198–200];
- FTP-75—EPA Federal Test Procedure [201–203];
- NEDC—New European Driving Cycle (NEDC) [204–206];
- US SC03—The SC03 (SFTP) [207,208];
- Random Cycle Low ( $\times 05$ )—a test generated from a procedure in the WLTP Random Cycle Generator tool [209,210];
- Random Cycle High ( $\times 95$ )—a test generated from a procedure in the WLTP Random Cycle Generator tool [211,212];
- MAC TP cycle—mobile air conditioning (MAC) [213,214];
- CADC—Artemis cycle definitions, includes the following cycles: urban, rural road and motorway [215–217];
- CADC w/o mot—Artemis cycle definitions, includes the following cycles: Urban, Rural Road. Does not include: Motorway [215–217];
- CADC abridged—same as Artemis cycle definitions, includes the following cycles: urban, rural road and motorway. The duration time was shortened, similar to CADC w/o mot [215–217];
- WLTC 3b random—WLTP for class 3 vehicles with the engine power above 34 W/kg [218–221].

Upon entering the complete information about the vehicle, the program is ready to generate the necessary waveforms in the time domain, which in turn enable the determination of the instantaneous operating parameters of the program in question. These waveforms were then exported to text files. The instantaneous waveforms of the following quantities were used in the further stages of the simulation: simulation time [s]; engine speed [rpm]; power produced by the engine [kW]; torque generated by the engine [Nm]—a value calculated on the basis of the engine rotational speed and engine power; gear number [-]; vehicle speed [km/h].

#### 2.4. Simulator

A driving test simulator was developed in OpenModelica v1.16.2, based on the analysis of the data created with the use of the “Gearshift calculation tool” programme, the results of the process of neural network structure optimization and the properties of the tested biofuels [222]. The simulator is made up of blocks that are responsible for individual functionalities, and its connection diagram is presented in Figure 5 below:

- Drive tests generator (text files)—responsible for loading files with data that control the selected driving test process from a text file created with the use of the “Gearshift calculation tool” application. It is also responsible for converting the read data to other formats compatible with OpenModelica v1.16.2. The following parameters are then relayed to the following calculation modules of the simulation: engine speed, engine torque, vehicle speed;
- Model of specific consumption (neural)—this block calculates the instantaneous values of petrol 95 mass flow and relays this parameter to the next block, based on the quantities which characterize the engine operating parameters: engine speed, engine torque and the prepared neural network structure;
- Calculations of fuel and CO<sub>2</sub> mass flows—this block is responsible for calculating the streams of the tested biofuels which are necessary to power the engine in the driving test. This is achieved using the petrol 95 mass flow parameter and the fuel calorific value characteristic for the fuel in question calculated in the previous block. This block also calculates the CO<sub>2</sub> emission stream with the use of the carbon mass content property and the instantaneous fuel stream;
- Calculation of driving test parameters—on the basis of the driving test parameters, this block calculates the distance covered by the vehicle during the test, the power generated by the engine and the mechanical energy generated during the test.

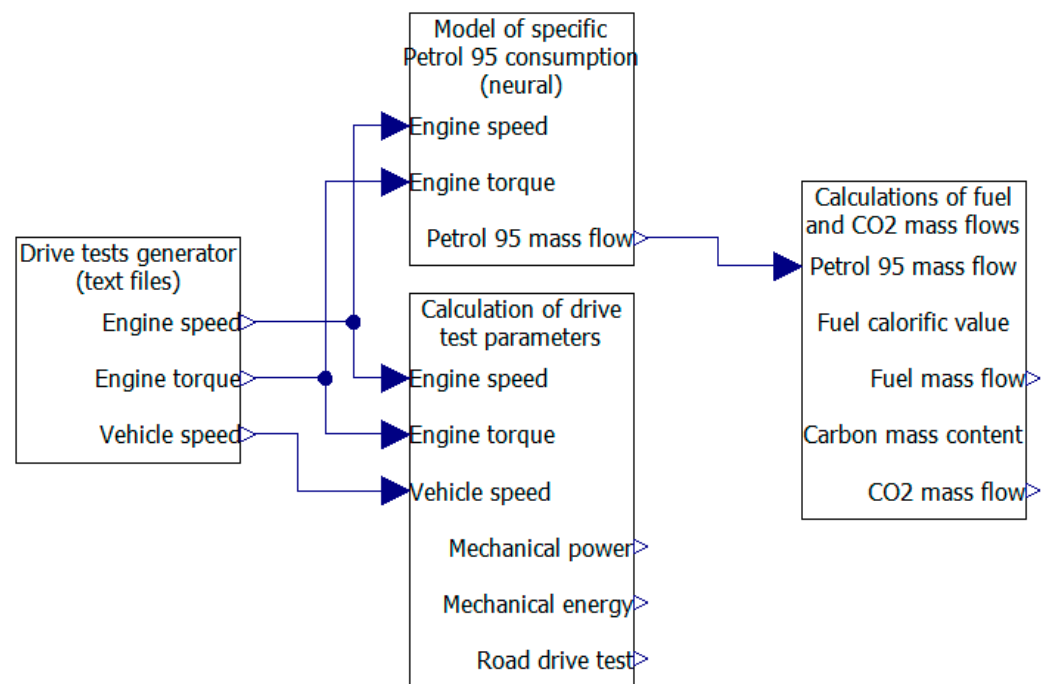


**Figure 5.** A general schematic of the driving test simulator, including biofuels OpenModelica v1.16.2 software.

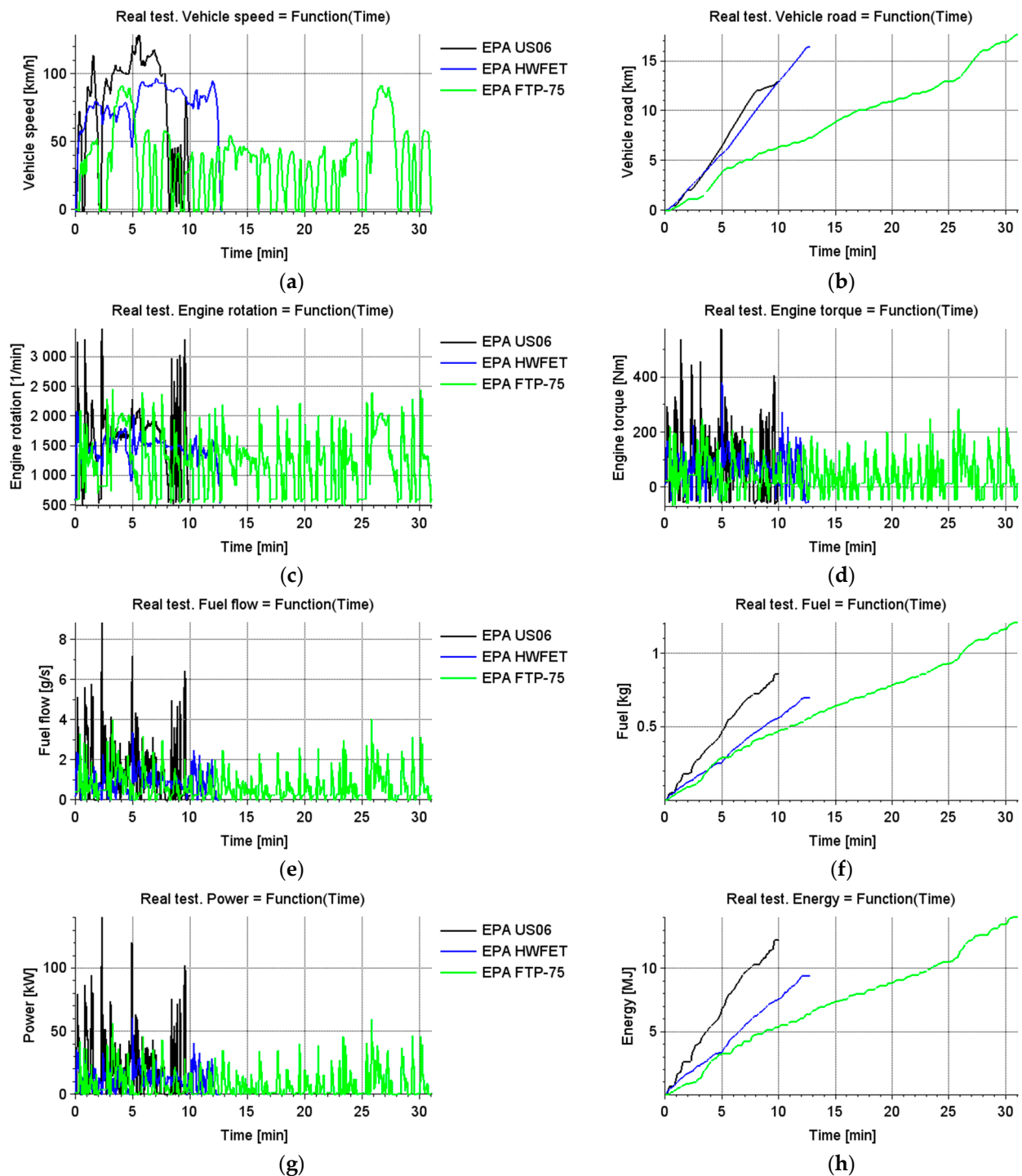
### 3. Results

Presented below are the processes of independent simulations of the selected Toyota Camry LE 2018 vehicle in the applied driving tests with changing fuels (petrol 95, ethanol, methanol, DME, CNG and LPG):

- the results of the simulation work for the processed EPA test data, which are learning models for the neural network;
- the results of the driving test simulator for the prepared drive tests (the “Gearshift Calculation Tool” application) in the form of vehicle speed graphs, distance travelled, engine speed, engine torque, engine power and mechanical energy used during the test;
- the simulation results for the stream and final fuel consumption;
- the simulation results for the stream and CO<sub>2</sub> emissions for selected driving tests and selected fuels for the 2018 Toyota Camry LE vehicle;
- the results of fuel consumption and carbon dioxide emissivity per 1 km of the distance travelled by the vehicle in the tests and per 1 kWh of the mechanical energy generated in the test.

#### 3.1. Simulation Work Results for the Processed EPA Test Data

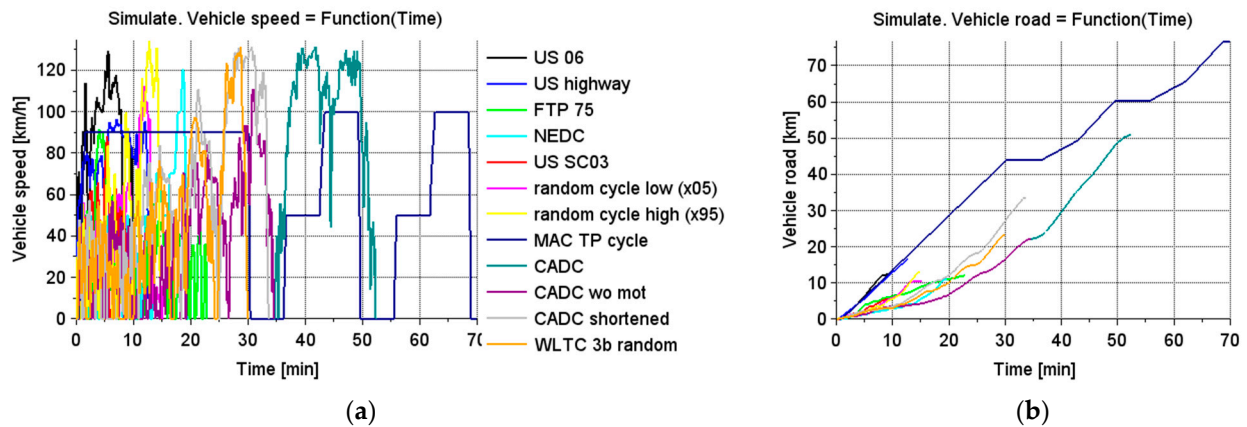
The published data from actual vehicle tests carried out by the EPA were used in order to verify the correct operation of the driving test simulator. The input data were so transformed that they could be fed into the simulator. As a result of the simulator’s work, the instantaneous values of the key simulation parameters were obtained, which are hereby presented in the figures below (Figure 6) [184].



**Figure 6.** The results of the simulation work for the processed data from EPA tests for the Toyota Camry LE 2018 vehicle: (a) waveforms of the instantaneous vehicle speed values; (b) waveforms of the instantaneous values of the distance travelled by the vehicle; (c) waveforms of the instantaneous vehicle engine speed values; (d) waveforms of the instantaneous values of torque generated by the vehicle engine; (e) waveforms of the instantaneous values of the fuel stream powering the vehicle engine; (f) waveforms of the instantaneous fuel consumption values for the vehicle; (g) waveforms of the instantaneous values of power generated by the vehicle's engine; (h) waveforms of the instantaneous values of mechanical energy generated by the vehicle engine.

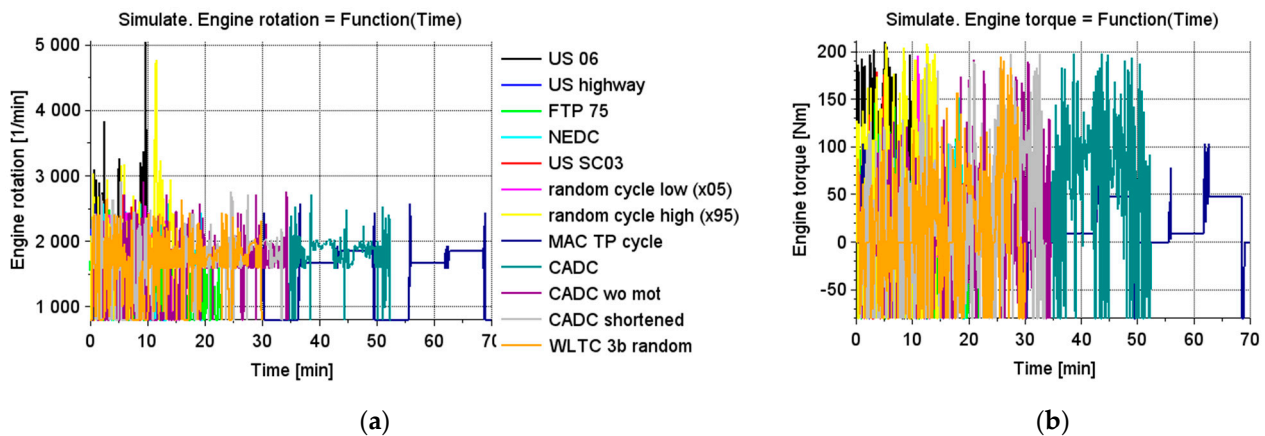
### 3.2. Simulation Work Results for the Driving Tests Performed

On the basis of the prepared input data, using the “Gearshift Calculation Tool” software, simulations of selected driving tests were carried out for the vehicle in question. Figure 7 below shows the waveforms of the instantaneous vehicle speed values in the test. These waveforms indicate a large variability of this parameter in the simulated tests, including mean values, the dynamics of changes and the changes in the distribution of the values over time. The simulated tests were also characterized by high variability of the execution time.



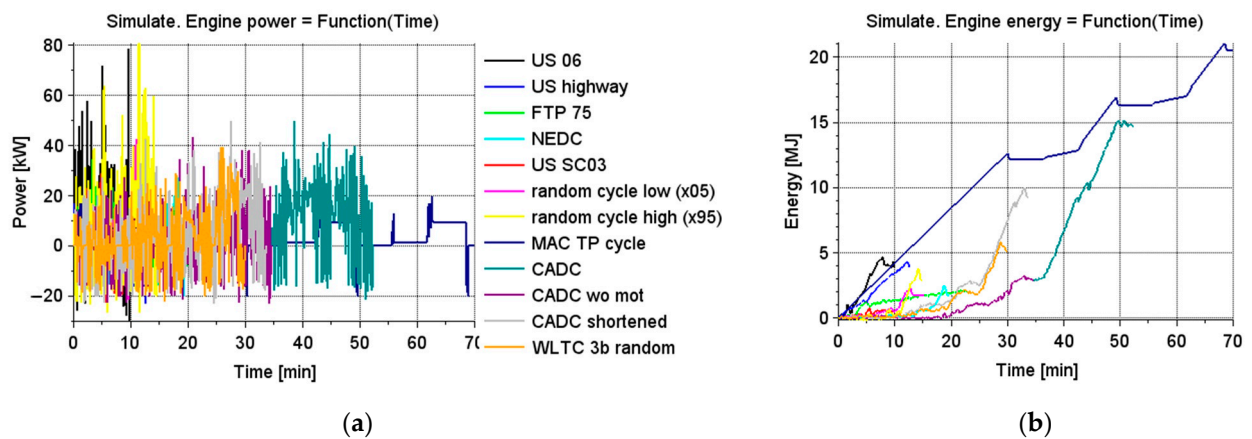
**Figure 7.** Results obtained in the simulation of selected road tests for the Toyota Camry LE 2018 vehicle: (a) waveforms of the instantaneous vehicle speed values; (b) waveforms of the instantaneous values of the distance travelled by the vehicle.

Figure 8 shows the waveforms of the instantaneous values of the travelled distance in the simulated tests in question. Other input parameters for the driving test simulator were the instantaneous values of the engine speed and the engine-generated torque, whose waveforms are presented below.



**Figure 8.** Results obtained in the simulation of selected road tests for the Toyota Camry LE 2018 vehicle: (a) waveforms of the instantaneous values of the vehicle engine rotational speed; (b) waveforms of the instantaneous values of the torque generated by the vehicle engine.

The instantaneous values of the power generated by the engine and the mechanical energy used during the test were calculated in the developed driving test simulator. Figure 9a,b show the waveforms of these parameters.



**Figure 9.** Results obtained in the simulation of selected road tests for the Toyota Camry LE 2018 vehicle: (a) waveforms of the instantaneous values of power generated by the engine; (b) waveforms of the instantaneous values of mechanical energy generated by the vehicle engine.

### 3.3. Simulation Results for the Stream and Final Fuel Consumption for the Selected Driving Tests and Fuels

The instantaneous values of fuel streams and their mass consumption for the tests in question were calculated on the basis of the values of the petrol 95 stream calculated in the simulator, taking into account the calorific values of the other considered fuels. The figures below (Figure 10) present a summary of the obtained waveforms of the instantaneous values of fuel flows and the mass consumption of fuels in the given driving test.

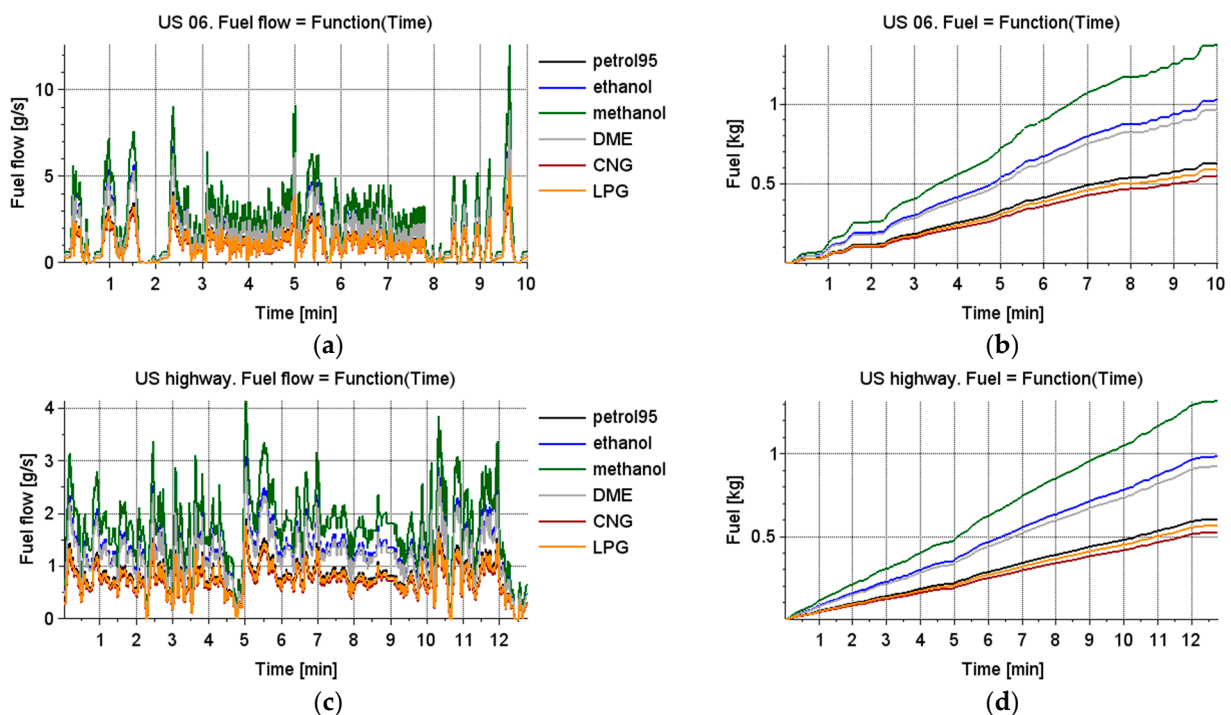


**Figure 10.** Cont.

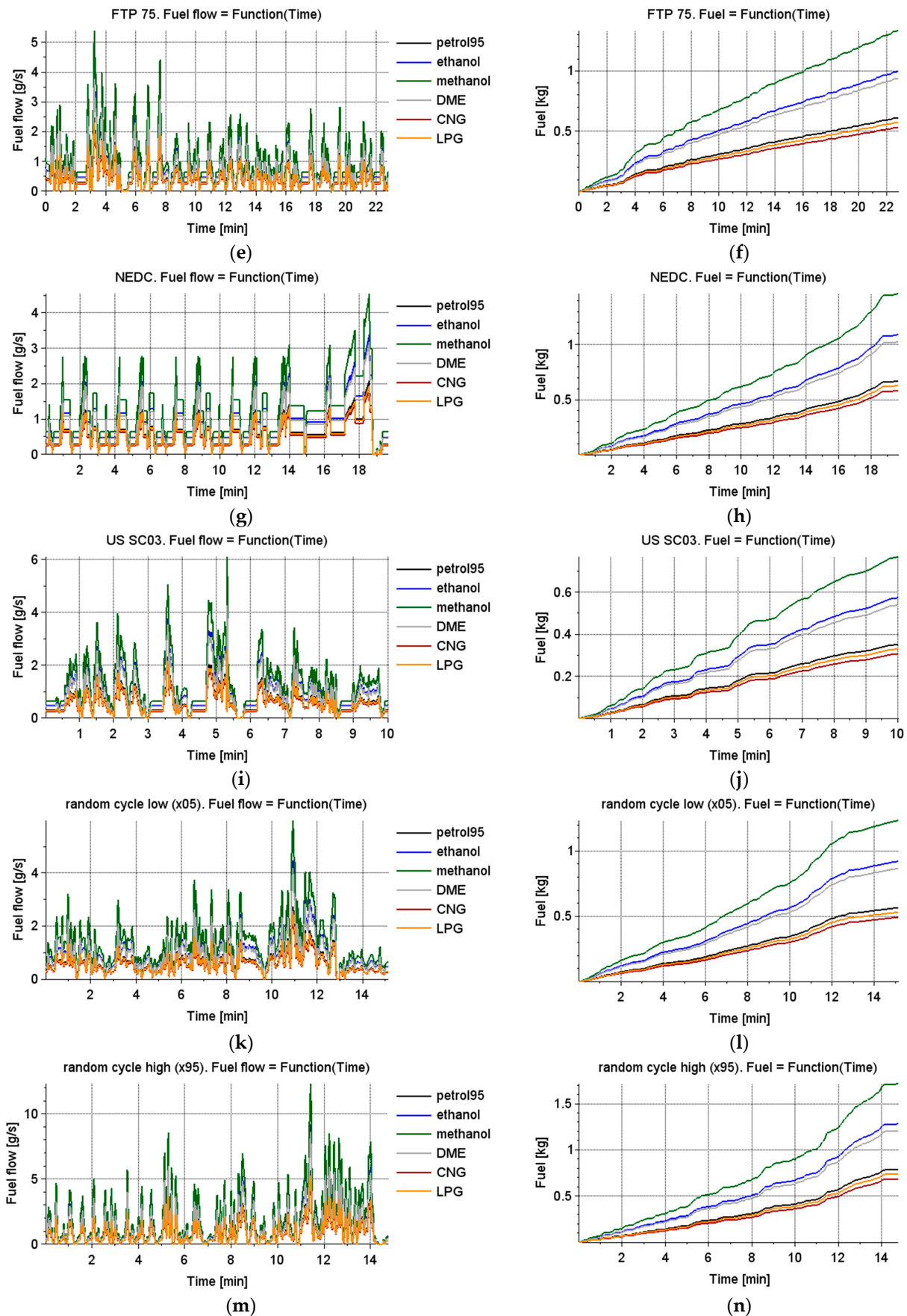
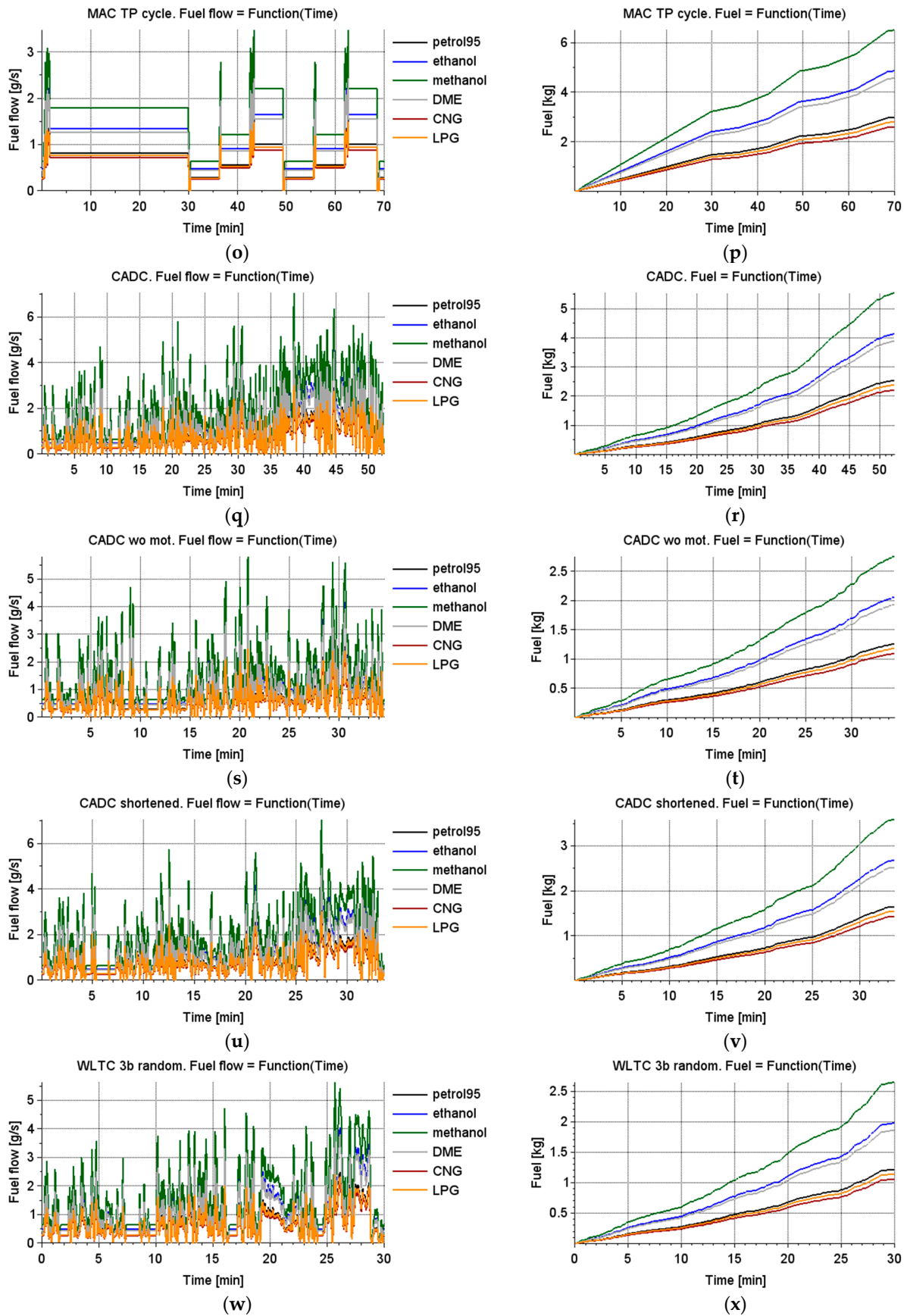


Figure 10. Cont.





**Figure 10.** Results of the simulation of the stream and final fuel consumption for selected driving tests and selected fuels for the Toyota Camry LE 2018 vehicle: (a) waveforms of the instantaneous values of the fuel stream powering the vehicle’s

engine, obtained in the simulation of the US 06 road test; (b) waveforms of the instantaneous values of fuel consumption for the vehicle, obtained in the simulation of the US 06 road test; (c) waveforms of the instantaneous values of the fuel stream powering the vehicle's engine, obtained in the simulation of the US highway road test; (d) waveforms of the instantaneous values fuel consumption values for the vehicle, obtained in the US highway test simulation; (e) waveforms of the instantaneous values of the fuel stream powering the vehicle's engine, obtained in the simulation of the FTP-75 road test; (f) waveforms of the instantaneous values of fuel consumption for the vehicle, obtained in the simulation of the FTP-75 road test; (g) waveforms of the instantaneous values of the fuel stream powering the vehicle's engine, obtained in the simulation of the New European Driving Cycle (NEDC) road test; (h) waveforms of the instantaneous values of fuel consumption for the vehicle, obtained in the simulation of the NEDC road test; (i) waveforms of the instantaneous values of the fuel stream powering the vehicle's engine, obtained in the simulation of the US SC03 road test; (j) waveforms of the instantaneous values of fuel consumption for the vehicle, obtained in the simulation of the US SC03 road test; (k) waveforms of the instantaneous values of the fuel stream powering the vehicle's engine, obtained in the simulation of the Random Cycle Low ( $\times 05$ ) road test; (l) waveforms of the instantaneous values of fuel consumption for the vehicle, obtained in the simulation of the Random Cycle Low ( $\times 05$ ) road test; (m) waveforms of the instantaneous values of the fuel stream powering the vehicle's engine, obtained in the simulation of the Random Cycle High ( $\times 95$ ) road test; (n) waveforms of the instantaneous values of the fuel consumption for the vehicle, obtained in the simulation of the Random Cycle High ( $\times 95$ ) road test; (o) waveforms of the instantaneous values of the fuel stream powering the vehicle's engine, obtained in the simulation of the Mobile Air Conditioning Test Procedure (MAC TP) cycle road test; (p) waveforms of the instantaneous values of fuel consumption for the vehicle, obtained in the simulation of the MAC TP cycle road test; (q) waveforms of the instantaneous values of the fuel stream powering the vehicle's engine, obtained in the simulation of the Common Artemis Driving Cycles (CADC) road test; (r) waveforms of the instantaneous values of fuel consumption for the vehicle, obtained in the simulation of the CADC road test; (s) waveforms of the instantaneous values of the fuel stream powering the vehicle's engine, obtained in the simulation of the CADC w/o mot road test; (t) waveforms of the instantaneous values of fuel consumption for the vehicle, obtained in the simulation of the CADC w/o mot road test; (u) waveforms of the instantaneous values of the fuel stream powering the vehicle's engine, obtained in the simulation of the CADC shortened road test; (v) waveforms of the instantaneous values of fuel consumption for the vehicle, obtained in the simulation of the CADC shortened road test; (w) waveforms of the instantaneous values of the fuel stream powering the vehicle's engine, obtained in the simulation of the Worldwide Harmonized Light-Duty Vehicles Test Cycles (WLTC) 3b random road test; (x) waveforms of the instantaneous values of fuel consumption for the vehicle, obtained in the simulation of the WLTC 3b random road test.

### 3.4. The Results of the Simulation of Carbon Dioxide Flux and Emissions for Selected Driving Tests and Fuels

As a result of the vehicle simulation processes performed for selected driving tests, including various fuels, the instantaneous values of the carbon dioxide flux and its emissivity during the test were obtained. The figures below (Figure 11) show the results of the simulator work in the form of the waveforms of carbon dioxide streams and its emissivity while taking into account the fuels considered for individual simulated tests.

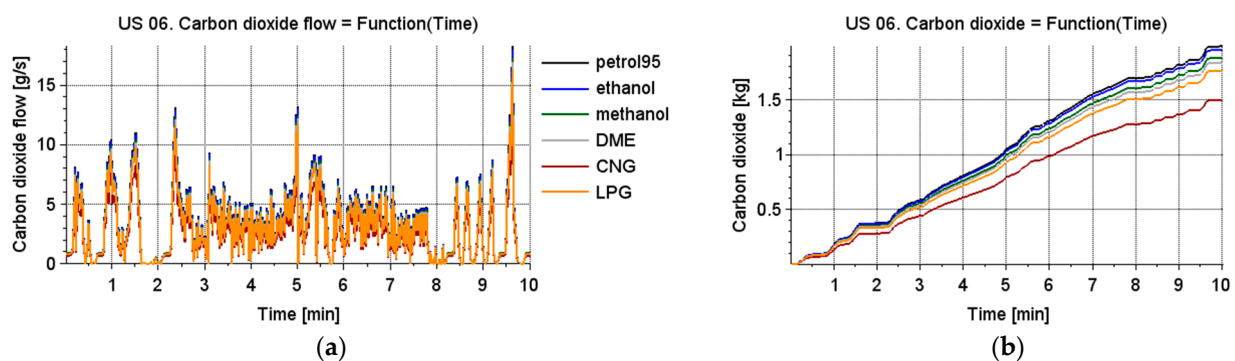


Figure 11. Cont.

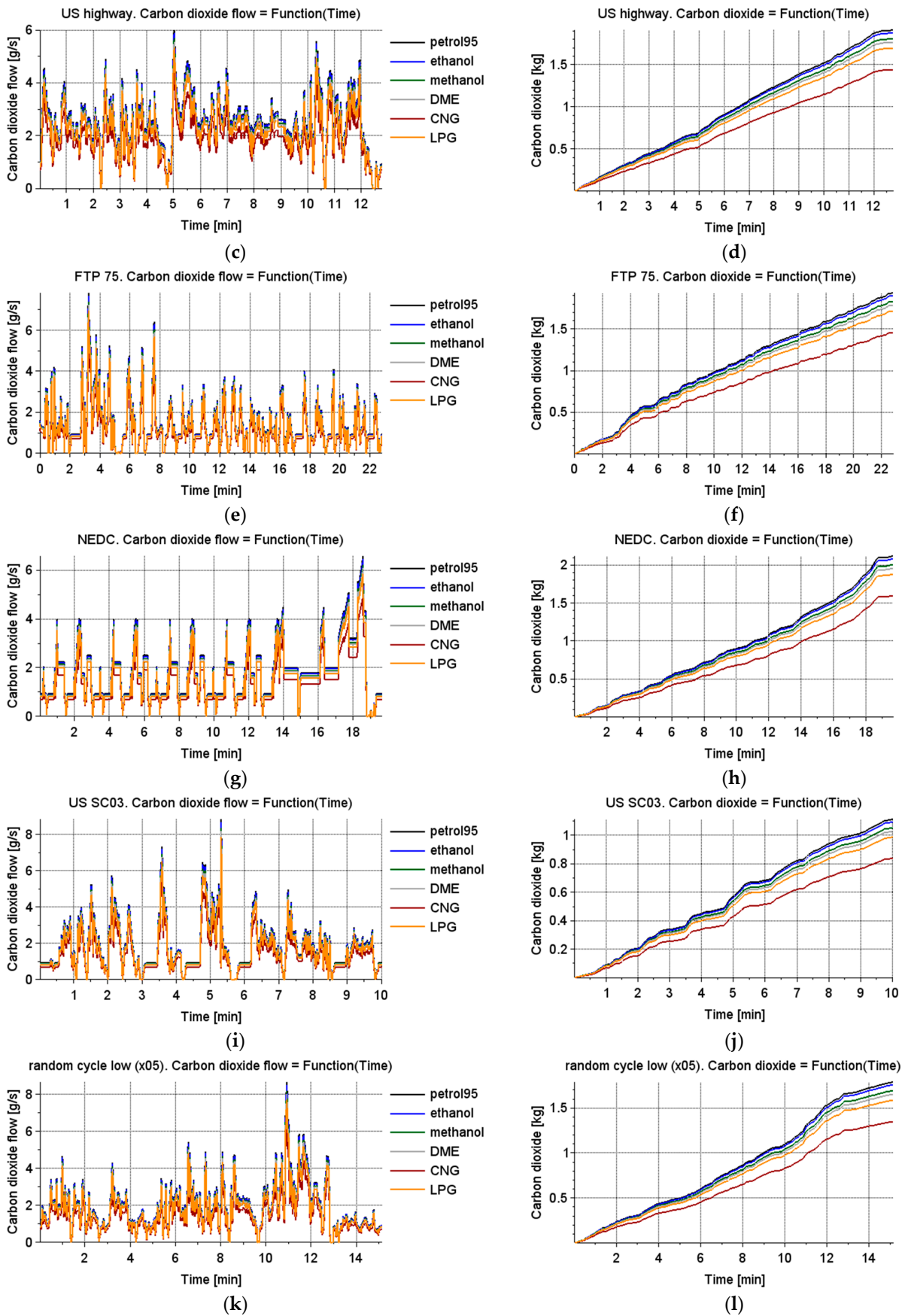


Figure 11. Cont.

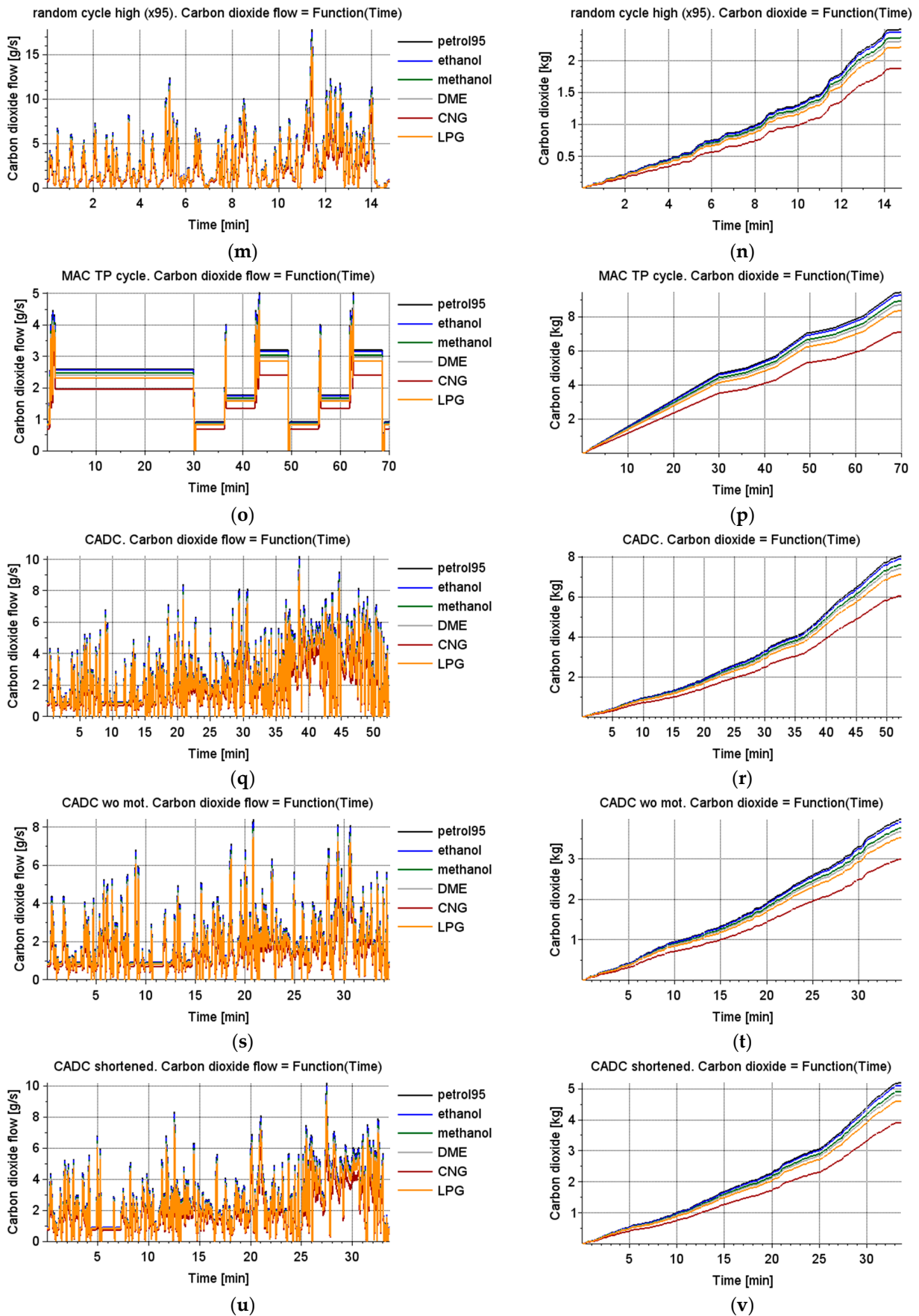
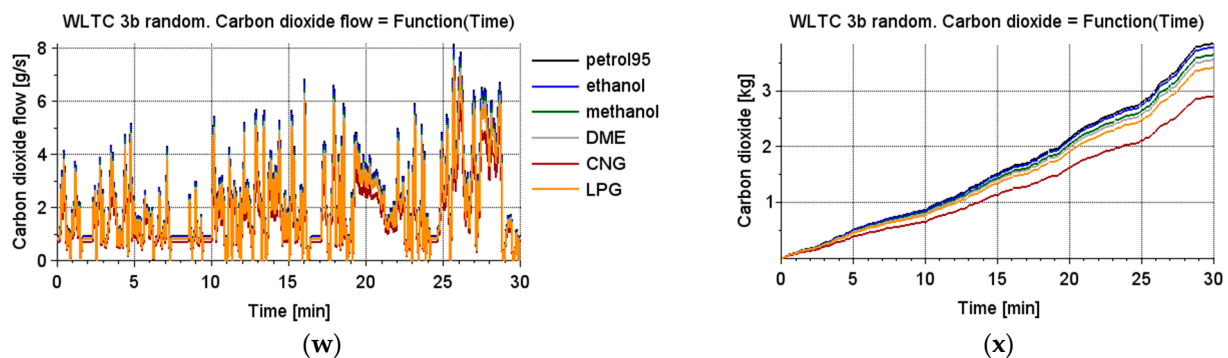


Figure 11. Cont.



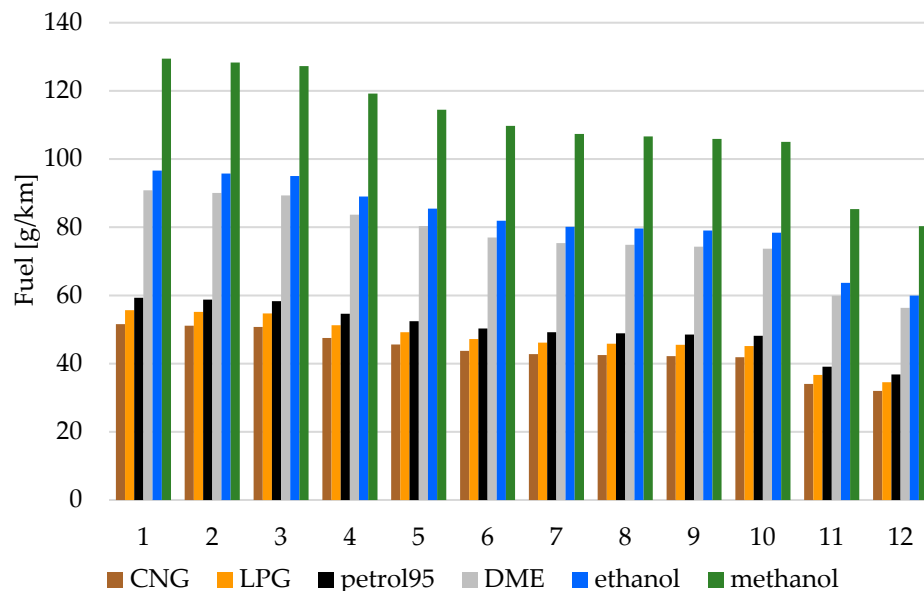
**Figure 11.** The results of the simulation of the carbon dioxide stream and emission for selected driving tests and fuels for the Toyota Camry LE 2018 vehicle: (a) waveforms of the instantaneous values of the carbon dioxide emission stream produced by the vehicle engine, obtained in the simulation of the US 06 road test; (b) waveforms of Table 06 road test; (c) waveforms of the instantaneous values of the carbon dioxide emission stream produced by the vehicle engine, obtained in the simulation of the US Highway road test; (d) waveforms of the instantaneous values of the carbon dioxide emission produced by the vehicle engine, obtained in the simulation of the US Highway road test; (e) waveforms of the instantaneous values of the carbon dioxide emission stream produced by the vehicle engine, obtained in the simulation of the FTP-75 road test; (f) waveforms of the instantaneous values of the carbon dioxide emission produced by the vehicle engine, obtained in the simulation of the FTP-75 road test; (g) waveforms of the instantaneous values of the carbon dioxide emission stream produced by the vehicle engine, obtained in the simulation of the NEDC road test; (h) waveforms of the instantaneous values of the carbon dioxide emission produced by the vehicle engine, obtained in the simulation of the US 06 road test; (i) waveforms of the instantaneous values of the carbon dioxide emission stream produced by the vehicle engine, obtained in the simulation of the US SC03 road test; (j) waveforms of the instantaneous values of the carbon dioxide emission produced by the vehicle engine, obtained in the simulation of the US SC03 road test; (k) waveforms of the instantaneous values of the carbon dioxide emission stream produced by the vehicle engine, obtained in the simulation of the Random Cycle Low road test ( $\times 05$ ); (l) waveforms of the instantaneous values of the carbon dioxide emission produced by the vehicle engine, obtained in the simulation of the Random Cycle Low road test ( $\times 05$ ); (m) waveforms of the instantaneous values of the carbon dioxide emission stream produced by the vehicle engine, obtained in the simulation of the Random Cycle High road test ( $\times 95$ ); (n) waveforms of the instantaneous values of the carbon dioxide emission produced by the vehicle engine, obtained in the simulation of the Random Cycle High ( $\times 95$ ) road test; (o) waveforms of the instantaneous values of the carbon dioxide emission stream produced by the vehicle engine, obtained in the simulation of the MAC TP road test; (p) waveforms of the instantaneous values of the carbon dioxide emission produced by the vehicle engine, obtained in the simulation of the MAC TP road test; (q) waveforms of the instantaneous values of the carbon dioxide emission stream produced by the vehicle engine, obtained in the simulation of the CADC road test; (r) waveforms of the instantaneous values of the carbon dioxide emission produced by the vehicle engine, obtained in the simulation of the CADC road test; (s) waveforms of the instantaneous values of the carbon dioxide emission stream produced by the vehicle engine, obtained in the simulation of the CADC w/o mot road test; (t) waveforms of the instantaneous values of the carbon dioxide emission produced by the vehicle engine, obtained in the simulation of the CADC w/o mot road test; (u) waveforms of the instantaneous values of the carbon dioxide emission stream produced by the vehicle engine, obtained in the simulation of the CADC shortened road test; (v) waveforms of the instantaneous values of the carbon dioxide emission produced by the vehicle engine, obtained in the simulation of the CADC shortened road test; (w) waveforms of the instantaneous values of the carbon dioxide emission stream produced by the vehicle engine, obtained in the simulation of the WLTC 3b random road test; (x) waveforms of the instantaneous values of the carbon dioxide emission produced by the vehicle engine, obtained in the simulation of the WLTC 3b road test.

#### 4. Discussion

The developed tool and the methodology used to build quantitative models of fuel consumption and CO<sub>2</sub> emissivity of the selected vehicle as a function of engine load and vehicle speed might constitute the basis for the construction of road simulators. In this case, the simulation tool can be adapted to the operational parameters of a large set of vehicles that represent a given car market. Road simulators developed on the basis of the described

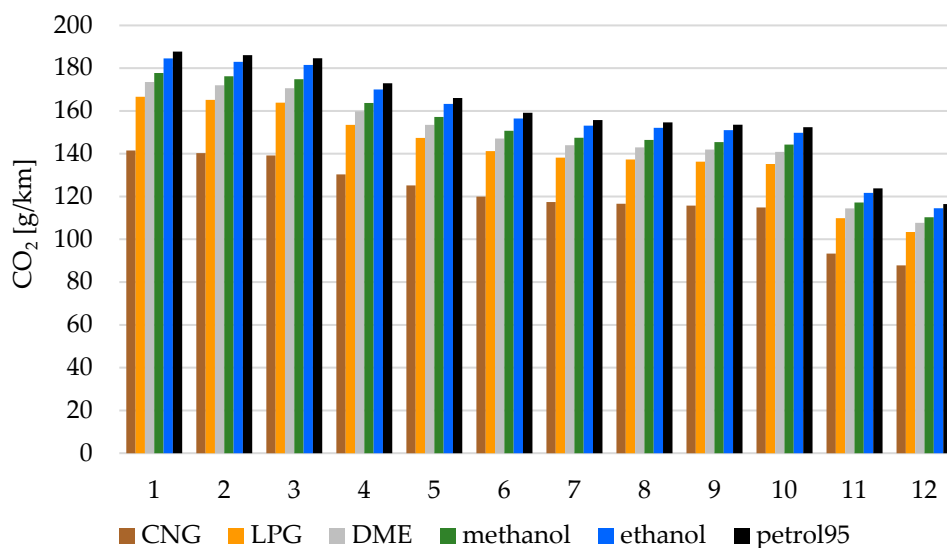
tool will make it possible to obtain more precise emissivity values in road traffic than the adopted environmental estimates.

Figure 12 presents the results of the simulator work for the considered fuels and driving tests in the form of the fuel consumption parameter per one kilometer driven in the test. For CNG fuel, the minimum value was achieved at the level of 32 g/km for the US highway test, while the maximum value was obtained at the random cycle high ( $\times 95$ ) (129.4 g/km) for methanol.



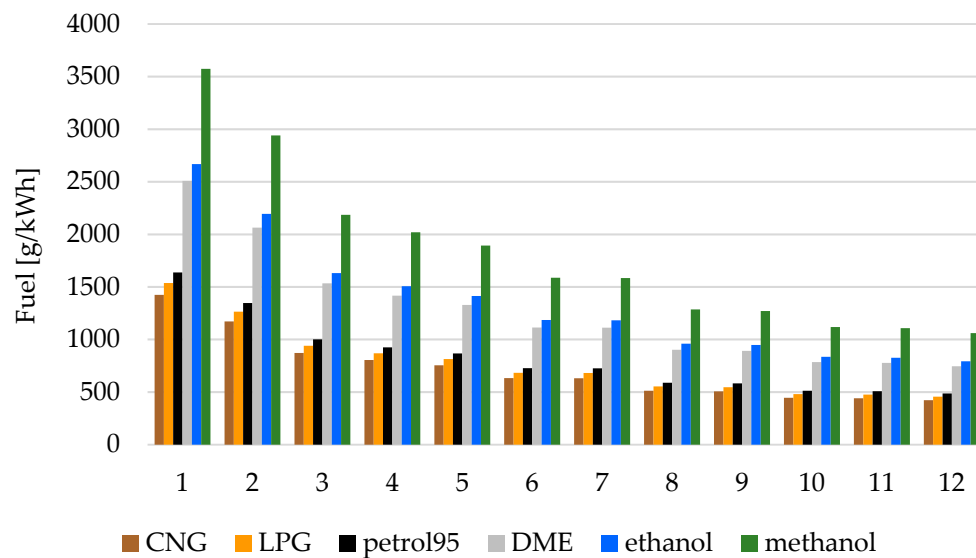
**Figure 12.** A summary of the mass consumption of the tested fuels per one kilometer driven: 1—Random cycle high ( $\times 95$ ); 2—NEDC; 3—US SC03; 4—CADC wo mot; 5—Random Cycle Low ( $\times 05$ ); 6—WLTC 3b random; 7—FTP-75; 8—CADC; 9—US 06; 10—CADC shortened; 11—MAC TP cycle; 12—US highway.

Figure 13 presents the results of the simulator work for the considered fuels and driving tests in the form of the CO<sub>2</sub> emission parameter per one kilometer driven in the test. For petrol 95, the minimum value was reached at 116 g/km for the US highway test, while the maximum value was obtained at the random cycle high ( $\times 95$ ) (187 g/km).



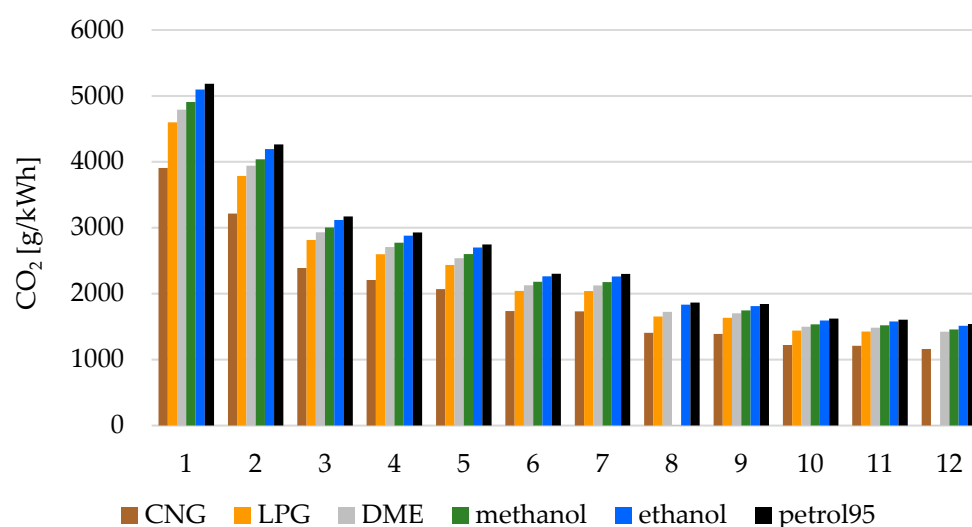
**Figure 13.** A summary of the carbon dioxide emission in the tests per one kilometer driven: 1—Random cycle high ( $\times 95$ ); 2—NEDC; 3—US SC03; 4—CADC wo mot; 5—Random Cycle Low ( $\times 05$ ); 6—WLTC 3b random; 7—FTP-75; 8—CADC; 9—US 06; 10—CADC shortened; 11—MAC TP cycle; 12—US highway.

Figure 14 below shows the data obtained from the performed simulations of driving tests, including biofuels, in the form of the parameter of mass consumption of a given fuel per unit of mechanical energy produced (1 kWh). For petrol 95, the minimum value was achieved at the level of 486 g/kWh for the US 06 driving test, while the maximum value was obtained for the US SC03 test (1630 g/kWh).



**Figure 14.** A summary of the fuel mass consumption in the tests per one kilowatt hour: 1—Random Cycle High ( $\times 95$ ); 2—NEDC; 3—US SC03; 4—CADC wo mot; 5—Random Cycle Low ( $\times 05$ ); 6—WLTC 3b random; 7—FTP-75; 8—CADC; 9—US 06; 10—CADC shortened; 11—MAC TP cycle; 12—US highway.

Figure 15 presents the results of the simulator work for the considered fuels and driving tests in the form of the carbon dioxide emission parameter per unit of mechanical energy produced (1 kilowatt-hour). For petrol 95, the minimum value was achieved at the level of 1538 g/kWh for the US 06 driving test, while the maximum value was obtained for the US SC03 (5182 g/kWh).



**Figure 15.** A Summary of carbon dioxide emissions in the tests per one kilowatt hour: 1—Random Cycle High ( $\times 95$ ); 2—NEDC; 3—US SC03; 4—CADC wo mot; 5—Random Cycle Low ( $\times 05$ ); 6—WLTC 3b random; 7—FTP-75; 8—CADC; 9—US 06; 10—CADC shortened; 11—MAC TP cycle; 12—US highway.

## 5. Conclusions

The paper presents a computer tool for simulating driving tests as a function of the consumption of selected fuels and biofuels and CO<sub>2</sub> emissivity, dedicated to vehicles with spark ignition engines. The basis for the work conducted was chassis dynamometer tests on the Toyota Camry LE 2018 vehicle.

- Neural network structures characterized by approximation (regression) properties were used to build a model enabling the determination of instantaneous fuel consumption values as a function of engine rotational speed and torque produced by the engine. The process of learning these network structures used data from actual driving tests performed on a selected vehicle on a chassis dynamometer published by the EPA. After selecting the neural network structure that obtained the smallest value of relative error with respect to the data from real measurements, the verification of the obtained neural model was carried out using the verification data of real tests included in the EPA publication.
- Based on the operational parameters analyzed with the use of the “Gearshift Calculation Tool” application, the results of the optimization process of the neural network structures and the properties of the biofuels in question, a driving test simulator was developed in the OpenModelica v1.16.2 program. Scilab 6.1.0 numerical software was then used to build the neural model.
- The developed simulation tool used neural networks, whose learning processes used the Levenberg–Marquardt algorithm. An optimization process was carried out for various investigated network structures differing in the number of input parameters and the number of neurons in the hidden layer. The relative error between the model and actual data did not exceed 1%.
- Twelve driving tests were analyzed in this study. These tests differed from one another in terms of the duration, speeds achieved by the vehicle and allowances for the use of any additional equipment in the vehicle (e.g., A/C).
- When analyzing the consumption parameter of a given fuel per one kilometer driven in the test, the best results were achieved for CNG fuel, for which the minimum value was reached at 32 g/km for the US highway driving test, while the maximum value was obtained in the Random Cycle High test (×95) (52.0 g/km). The highest fuel consumption per one kilometer in the test was observed in the case of methanol in the Random Cycle High (×95) (129.4 g/km).
- When considering the emissions of carbon dioxide per kilometer in the test, the highest values were recorded for petrol 95, where the minimum value was reached at 116 g/km for the US highway driving test, and the maximum value was obtained at a Random Cycle High (×95) (187 g/km). For CNG, the minimum value was reached for the US highway (87.7 g/km).
- When analyzing the parameter of mass consumption of a given fuel per unit of mechanical energy produced (1 kilowatt hour) in the case of petrol 95, the minimum value was achieved at 486 g/kWh for the US 06 driving test, while the maximum value was obtained for the US SC03 (1630 g/kWh). The highest consumption was recorded for US SC03, also for DME (2507 g/kWh), ethanol (2667 g/kWh) and methanol (3573 g/kWh).
- For the parameter of carbon dioxide emission per unit of mechanical energy produced (1 kilowatt hour), the maximum values were obtained for US SC03 CNG (3906 g/kWh), LPG (4599 g/kWh), DME (4790 g/kWh), methanol (4907 g/kWh), ethanol (5095 g/kWh) and petrol 95 (5182 g/kWh).
- The developed computer tool could be the basis for the development of a method of identifying selected aspects of operating conditions and assessing the energy efficiency of vehicles with spark ignition engines powered by fuels and biofuels.
- The research method described in the manuscript aims to obtain a simulation model to calculate instantaneous fuel consumption as a function of engine speed and engine torque produced. This method allows the simulation of vehicle operations under



different load conditions and will potentially allow the calculation of fuel consumption and carbon emissions. This method can be used for many popular vehicle models in a given market. In the case of estimating carbon dioxide emissions for real facilities where vehicles move, e.g., road tunnels and large parking lots, a very large number of simulations of individual vehicles in real traffic can be used in a single simulation. The use of such simulations will allow for the more precise selection of ventilation systems for such objects, which will prevent the increase in carbon dioxide content in the air.

**Funding:** The APC was funded by Institute of Mechanical Engineering, Warsaw University of Life Sciences.

**Institutional Review Board Statement:** Not applicable.

**Informed Consent Statement:** Not applicable.

**Data Availability Statement:** All data are presented in this article. Data sharing is not applicable to this article.

**Conflicts of Interest:** The author declares no conflict of interests.

## References

1. Beaudet, A.; Larouche, F.; Amouzegar, K.; Bouchard, P.; Zaghib, K. Key Challenges and Opportunities for Recycling Electric Vehicle Battery Materials. *Sustainability* **2020**, *12*, 5837. [CrossRef]
2. Krysko, A.V.; Awrejcewicz, J.; Pavlov, S.P.; Bodyagina, K.S.; Krysko, V.A. Topological optimization of thermoelastic composites with maximized stiffness and heat transfer. *Compos. Part B Eng.* **2019**, *158*, 319–327. [CrossRef]
3. Pawełko, P.; Berczyński, S.; Grządziel, Z. Modeling roller guides with preload. *Arch. Civ. Mech. Eng.* **2014**, *14*, 691–699. [CrossRef]
4. Nabagło, T.; Kowal, J.; Jurkiewicz, A. High Fidelity Model Construction and Its Verification Based on 2S1 Tracked Vehicle. In *Innovative Control Systems for Tracked Vehicle Platforms. Studies in Systems, Decision and Control. Part III: Construction and Investigation of the Dynamic Characteristics of Tracked Vehicles*, 1st ed.; Nawrat, M.A., Ed.; Springer: Cham, Switzerland, 2015; Volume 2, pp. 205–215.
5. Maizak, D.; Wilberforce, T.; Olabi, A.G. DeNOx removal techniques for automotive applications—A review. *Environ. Adv.* **2020**, *2*, 100021. [CrossRef]
6. Ogunkunle, O.; Ahmed, N.A. Exhaust emissions and engine performance analysis of a marine diesel engine fuelled with Parinari polyandra biodiesel–diesel blends. *Energy Rep.* **2020**, *6*, 2999–3007. [CrossRef]
7. Olabi, A.G.; Wilberforce, T.; Abdelkareem, M.A. Fuel cell application in the automotive industry and future perspective. *Energy* **2021**, *214*, 118955. [CrossRef]
8. Kumar, M.S.; Prabhakar, M.; Sendilvelan, S.; Singh, S.; Venkatesh, R.; Bhaskar, K. Combustion, performance and emission analysis of a diesel engine fueled with methyl esters of Jatropha and fish oil with exhaust gas recirculation. *Energy Procedia* **2019**, *160*, 404–411. [CrossRef]
9. Ang, J.G.; Fredriksson, P.G. Does an early start help or hurt? Statehood, institutions and modern climate change policies. *Energy Econ.* **2021**, *94*, 105075. [CrossRef]
10. Fekete, H.; Kuramochi, T.; Roelfsema, M.; Den Elzen, M.; Forsell, N.; Höhne, N.; Luna, L.; Hans, F.; Sterl, S.; Olivier, J.; et al. A review of successful climate change mitigation policies in major emitting economies and the potential of global replication. *Renew. Sustain. Energy Rev.* **2021**, *137*, 110602. [CrossRef]
11. Enzmann, J.; Ringel, M. Reducing Road Transport Emissions in Europe: Investigating A Demand Side Driven Approach †. *Sustainability* **2020**, *12*, 7594. [CrossRef]
12. Coelho, S.; Rafael, S.; Lopes, D.; Miranda, A.I.; Ferreira, J. How changing climate may influence air pollution control strategies for 2030? *Sci. Total Environ.* **2021**, *758*, 143911. [CrossRef]
13. Brodny, J.; Tutak, M. The analysis of similarities between the European Union countries in terms of the level and structure of the emissions of selected gases and air pollutants into the atmosphere. *J. Clean. Prod.* **2021**, *279*, 123641. [CrossRef] [PubMed]
14. Nikas, A.; Gambhir, A.; Trutnevyte, E.; Koasidis, K.; Lund, H.; Thellufsen, J.Z.; Mayer, D.; Zachmann, G.; Miguel, L.J.; Ferreras-Alonso, N.; et al. Perspective of comprehensive and comprehensible multi-model energy and climate science in Europe. *Energy* **2021**, *215*, 119153. [CrossRef]
15. Cadillo-Benalcazar, J.J.; Bukkens, S.G.F.; Ripa, M.; Giampietro, M. Why does the European Union produce biofuels? Examining consistency and plausibility in prevailing narratives with quantitative storytelling. *Energy Res. Soc. Sci.* **2021**, *71*, 101810. [CrossRef]
16. CO<sub>2</sub> Emissions from Cars: Facts and Figures (Infographics). Available online: <https://www.europarl.europa.eu/news/en/headlines/society/20190313STO31218/co2-emissions-from-cars-facts-and-figures-infographics> (accessed on 23 January 2021).

17. McKinsey & Company. Carbon-Neutral Poland 2050. Available online: <https://www.mckinsey.com/pl/our-insights/carbon-neutral-poland-2050> (accessed on 23 January 2021).
18. European Parliament Approves Post-2020 CO<sub>2</sub> Emission Targets for Cars and Vans. Available online: <https://ihsmarkit.com/research-analysis/european-parliament-approves-post2020-co2-emission-targets.html> (accessed on 23 January 2021).
19. AECC Newsletter March 2019. Available online: <https://www.aecc.eu/wp-content/uploads/2019/04/AECC-Newsletter-March-2019.pdf> (accessed on 23 January 2021).
20. Transport. Available online: [https://www.ipcc.ch/site/assets/uploads/2018/02/ipcc\\_wg3\\_ar5\\_chapter8.pdf](https://www.ipcc.ch/site/assets/uploads/2018/02/ipcc_wg3_ar5_chapter8.pdf) (accessed on 23 January 2021).
21. Jing, R.; Yuan, C.; Rezaei, H.; Qian, J.; Zhang, Z. Assessments on energy and greenhouse gas emissions of internal combustion engine automobiles and electric automobiles in the USA. *J. Environ. Sci.* **2020**, *90*, 297–309. [[CrossRef](#)] [[PubMed](#)]
22. Akhshik, M.; Panthapulakkal, S.; Tjong, J.; Bilton, A.; Singh, C.V.; Sain, M. Cross-country analysis of life cycle assessment-based greenhouse gas emissions for automotive parts: Evaluation of coefficient of country. *Renew. Sustain. Energy Rev.* **2021**, *138*, 110546. [[CrossRef](#)]
23. Daziano, R.; Waygood, E.O.D.; Patterson, Z.; Feinberg, M.; Wang, B. Reframing greenhouse gas emissions information presentation on the Environmental Protection Agency's new-vehicle labels to increase willingness to pay. *J. Clean. Prod.* **2021**, *279*, 123669. [[CrossRef](#)]
24. Neupane, B.; Rubin, J. Implications of U.S. biofuels policy for sustainable transportation energy in Maine and the Northeast. *Renew. Sustain. Energy Rev.* **2017**, *70*, 729–735. [[CrossRef](#)]
25. Fast Facts on Transportation Greenhouse Gas Emissions. Available online: <https://www.epa.gov/greenvehicles/fast-facts-transportation-greenhouse-gas-emissions> (accessed on 23 January 2021).
26. Shahiduzzaman, M.; Layton, A. Decomposition analysis for assessing the United States 2025 emissions target: How big is the challenge? *Renew. Sustain. Energy Rev.* **2017**, *67*, 372–383. [[CrossRef](#)]
27. An Overview of Automotive Vehicle and Component Regulations in China. Available online: <https://incompliancemag.com/article/an-overview-of-automotive-vehicle-and-component-regulations-in-china/> (accessed on 23 January 2021).
28. Yan, X.; Crookes, R.J. Energy demand and emissions from road transportation vehicles in China. *Prog. Energy Combust. Sci.* **2010**, *36*, 651–676. [[CrossRef](#)]
29. Liu, Y.; Wu, Z.X.; Zhou, H.; Zheng, H.; Yu, N.; An, X.P.; Li, J.Y.; Li, M.L. Development of China Light-Duty Vehicle Test Cycle. *Int. J. Automot. Technol.* **2020**, *21*, 1233–1246. [[CrossRef](#)]
30. Liu, Y.; Zhou, H.; Xu, Y.; Qin, K.; Yu, H. *Feasibility Study of Using WLTC for Fuel Consumption Certification of Chinese Light-Duty Vehicles*; SAE Technical Paper 2018-01-0654; SAE International: Warrendale, PA, USA, 2018.
31. Wei, L.; Li, H.; Zhang, H.; Sun, S. The Analysis of CO<sub>2</sub> Emissions and Reduction Potential in China's Transport Sector. *Mathematical Problems in Engineering*. 2016, p. 1043717. Available online: <https://www.hindawi.com/journals/mpe/2016/1043717/> (accessed on 23 January 2021).
32. Zheng, Y.; Li, S.; Xu, S. Transport Oil Product Consumption and GHG Emission Reduction Potential in China: An Electric Vehicle-Based Scenario Analysis. Available online: <https://journals.plos.org/plosone/article?id=10.1371/journal.pone.0222448> (accessed on 23 January 2021).
33. Sustainable Transport in China. Available online: <https://www.sustainabletransport.org/archives/tag/carbon-emissions> (accessed on 23 January 2021).
34. Li, X.; Yu, B. Peaking CO<sub>2</sub> emissions for China's urban passenger transport sector. *Energy Policy* **2019**, *133*, 110913. [[CrossRef](#)]
35. Borucka, A.; Wiśniowski, P.; Mazurkiewicz, D.; Świdorski, A. Laboratory measurements of vehicle exhaust emissions in conditions reproducing real traffic. *Measurement* **2021**, *174*, 108998. [[CrossRef](#)]
36. Gao, J.; Chen, H.; Li, Y.; Chen, J.; Zhang, Y.; Dave, K.; Huang, Y. Fuel consumption and exhaust emissions of diesel vehicles in worldwide harmonized light vehicles test cycles and their sensitivities to eco-driving factors. *Energy Convers. Manag.* **2019**, *196*, 605–613. [[CrossRef](#)]
37. Sarkan, B.; Stopka, O.; Gnap, J.; Caban, J. Investigation of Exhaust Emissions of Vehicles with the Spark Ignition Engine within Emission Control. *Procedia Eng.* **2017**, *187*, 775–782. [[CrossRef](#)]
38. Xing, J.; Shao, L.; Zhang, W.; Peng, J.; Wang, W.; Hou, C.; Shuai, S.; Hu, M.; Zhang, D. Morphology and composition of particles emitted from a port fuel injection gasoline vehicle under real-world driving test cycles. *J. Environ. Sci.* **2019**, *76*, 339–348. [[CrossRef](#)] [[PubMed](#)]
39. Koossalapeerom, T.; Satiennam, T.; Satiennam, W.; Leelapatra, W.; Seedam, A.; Rakpukdee, T. Comparative study of real-world driving cycles, energy consumption, and CO<sub>2</sub> emissions of electric and gasoline motorcycles driving in a congested urban corridor. *Sustain. Cities Soc.* **2019**, *45*, 619–627. [[CrossRef](#)]
40. Wang, Y.; Hao, C.; Ge, Y.; Hao, L.; Tan, J.; Wang, X.; Zhang, P.; Wang, Y.; Tian, W.; Lin, Z.; et al. Fuel consumption and emission performance from light-duty conventional/hybrid-electric vehicles over different cycles and real driving tests. *Fuel* **2020**, *278*, 118340. [[CrossRef](#)]
41. Hagino, H.; Oyama, M.; Sasaki, S. Laboratory testing of airborne brake wear particle emissions using a dynamometer system under urban city driving cycles. *Atmos. Environ.* **2016**, *131*, 269–278. [[CrossRef](#)]

42. Wihersaari, H.; Pirjola, L.; Karjalainen, P.; Saukko, E.; Kuuluvainen, H.; Kulmala, K.; Keskinen, J.; Rönkkö, T. Particulate emissions of a modern diesel passenger car under laboratory and real-world transient driving conditions. *Environ. Pollut.* **2020**, *265*, 114948. [[CrossRef](#)]
43. Davari, M.M.; Jerrelind, J.; Trigell, A.S. Energy efficiency analyses of a vehicle in modal and transient driving cycles including longitudinal and vertical dynamics. *Transp. Res. Part D Transp. Environ.* **2017**, *53*, 263–275. [[CrossRef](#)]
44. Triantafyllopoulos, G.; Dimaratos, A.; Ntziachristos, L.; Bernard, Y.; Dornoff, J.; Samaras, Z. A study on the CO<sub>2</sub> and NO<sub>x</sub> emissions performance of Euro 6 diesel vehicles under various chassis dynamometer and on-road conditions including latest regulatory provisions. *Sci. Total Environ.* **2019**, *666*, 337–346. [[CrossRef](#)]
45. Chen, L.; Wang, Z.; Liu, S.; Qu, L. Using a chassis dynamometer to determine the influencing factors for the emissions of Euro VI vehicles. *Transp. Res. Part D Transp. Environ.* **2018**, *65*, 564–573. [[CrossRef](#)]
46. Lohse-Busch, H.; Stutenberg, K.; Duoba, M.; Liu, X.; Elgowainy, A.; Wang, M.; Wallner, T.; Richard, B.; Christenson, M. Automotive fuel cell stack and system efficiency and fuel consumption based on vehicle testing on a chassis dynamometer at minus 18 °C to positive 35 °C temperatures. *Int. J. Hydrogen Energy* **2020**, *45*, 861–872. [[CrossRef](#)]
47. Zhu, G.; Liu, F.J.; Xu, Z.; Guo, Q.; Zhao, H. Experimental study on combustion and emission characteristics of turbocharged gasoline direct injection (GDI) engine under cold start new European driving cycle (NEDC). *Fuel* **2015**, *215*, 272–284. [[CrossRef](#)]
48. Armas, O.; García-Contreras, R.; Ramos, A. Pollutant emissions from New European Driving Cycle with ethanol and butanol diesel blends. *Fuel Process. Technol.* **2014**, *122*, 64–71. [[CrossRef](#)]
49. Degraeuwe, B.; Weiss, M. Does the New European Driving Cycle (NEDC) really fail to capture the NO<sub>x</sub> emissions of diesel cars in Europe? *Environ. Pollut.* **2017**, *222*, 234–241. [[CrossRef](#)] [[PubMed](#)]
50. Ramos, A.; Muñoz, J.; Andrés, F.; Armas, O. NO<sub>x</sub> emissions from diesel light duty vehicle tested under NEDC and real-world driving conditions. *Transp. Res. Part D Transp. Environ.* **2018**, *63*, 37–48. [[CrossRef](#)]
51. Fontaras, G.; Valverde, V.; Arcidiacono, V.; Tsiakmakis, S.; Anagnostopoulos, K.; Komnos, D.; Pavlovic, J.; Ciuffo, B. The development and validation of a vehicle simulator for the introduction of Worldwide Harmonized test protocol in the European light duty vehicle CO<sub>2</sub> certification process. *Appl. Energy* **2018**, *226*, 784–796. [[CrossRef](#)]
52. Tsiakmakis, S.; Fontaras, G.; Anagnostopoulos, K.; Ciuffo, B.; Pavlovic, J.; Marotta, A. A simulation based approach for quantifying CO<sub>2</sub> emissions of light duty vehicle fleets. A case study on WLTP introduction. *Transp. Res. Procedia* **2017**, *25*, 3898–3908. [[CrossRef](#)]
53. Massaguer, E.; Massaguer, A.; Pujol, T.; Comamala, M.; Montoro, L.; Gonzalez, J.R. Fuel economy analysis under a WLTP cycle on a mid-size vehicle equipped with a thermoelectric energy recovery system. *Energy* **2019**, *179*, 306–314. [[CrossRef](#)]
54. The Introduction of the WLTP into the European Type-Approval for Light-Duty Vehicles. Available online: [https://ec.europa.eu/jrc/sites/jrcsh/files/wltp\\_20oct-morning\\_1.pdf](https://ec.europa.eu/jrc/sites/jrcsh/files/wltp_20oct-morning_1.pdf) (accessed on 27 January 2021).
55. Tutuianu, M.; Bonnel, P.; Ciuffo, B.; Haniu, T.; Ichikawa, N.; Marotta, A.; Pavlovic, J.; Steven, H. Development of the World-wide harmonized Light duty Test Cycle (WLTC) and a possible pathway for its introduction in the European legislation. *Transp. Res. Part D Transp. Environ.* **2015**, *40*, 61–75. [[CrossRef](#)]
56. Dimaratos, A.; Tsokolis, D.; Fontaras, G.; Tsiakmakis, S.; Ciuffo, B.; Samaras, Z. Comparative Evaluation of the Effect of Various Technologies on Light-duty Vehicle CO<sub>2</sub> Emissions over NEDC and WLTP. *Transp. Res. Procedia* **2016**, *14*, 3169–3178. [[CrossRef](#)]
57. Duarte, G.O.; Gonçalves, G.A.; Farias, T.L. Analysis of fuel consumption and pollutant emissions of regulated and alternative driving cycles based on real-world measurements. *Transp. Res. Part D Transp. Environ.* **2016**, *44*, 43–54. [[CrossRef](#)]
58. From NEDC to WLTP: What Will Change? Available online: <https://www.wltpfacts.eu/from-nedc-to-wltp-change/> (accessed on 27 January 2021).
59. Abdelkareem, M.A.A.; Xu, L.; Guo, X.; Ali, M.K.A.; Elagouz, A.; Hassan, M.A.; Essa, F.A.; Zou, J. Energy harvesting sensitivity analysis and assessment of the potential power and full car dynamics for different road modes. *Mech. Syst. Signal Process.* **2018**, *110*, 307–332. [[CrossRef](#)]
60. Björnsson, L.H.; Karlsson, S. The potential for brake energy regeneration under Swedish conditions. *Appl. Energy* **2016**, *168*, 75–84. [[CrossRef](#)]
61. Global WLTP Roll-Out for More Realistic Results in Fuel Consumption. Available online: <https://www.vda.de/en/topics/environment-and-climate/Global-WLTP-roll-out-for-more-realistic-results-in-fuel-consumption/WLTP-How-realistic-is-the-WLTP.html> (accessed on 27 January 2021).
62. WLTP Driving Cycle. Available online: <https://www.vauxhall.co.uk/wltp.html> (accessed on 27 January 2021).
63. Wang, S.; Li, Y.; Fu, J.; Liu, J.; Dong, H. Numerical research on the performance, combustion and energy flow characteristics of gasoline-powered vehicle under WLTC. *Fuel* **2021**, *285*, 119135. [[CrossRef](#)]
64. Karagöz, Y. Analysis of the impact of gasoline, biogas and biogas + hydrogen fuels on emissions and vehicle performance in the WLTC and NEDC. *Int. J. Hydrogen Energy* **2019**, *44*, 31621–31632. [[CrossRef](#)]
65. Sileghem, L.; Bosteels, D.; May, J.; Favre, C.; Verhelst, S. Analysis of vehicle emission measurements on the new WLTC, the NEDC and the CADC. *Transp. Res. Part D Transp. Environ.* **2014**, *32*, 70–85. [[CrossRef](#)]
66. Zachiotis, A.T.; Giakoumis, E.G. Non-regulatory parameters effect on consumption and emissions from a diesel-powered van over the WLTC. *Transp. Res. Part D Transp. Environ.* **2019**, *74*, 104–123. [[CrossRef](#)]
67. Wang, Y.; Ge, Y.; Wang, J.; Wang, X.; Yin, H.; Hao, L.; Tan, J. Impact of altitude on the real driving emission (RDE) results calculated in accordance to moving averaging window (MAW) method. *Fuel* **2020**, *277*, 117929. [[CrossRef](#)]

68. Kurtyka, K.; Pielecha, J. The evaluation of exhaust emission in RDE tests including dynamic driving conditions. *Transp. Res. Procedia* **2019**, *40*, 338–345. [CrossRef]
69. García-Contreras, R.; Soriano, J.A.; Fernández-Yáñez, P.; Sánchez-Rodríguez, L.; Mata, C.; Gómez, A.; Armas, O.; Cárdenas, M.D. Impact of regulated pollutant emissions of Euro 6d-Temp light-duty diesel vehicles under real driving conditions. *J. Clean. Prod.* **2021**, *286*, 124927. [CrossRef]
70. Expectations for Actual Euro 6 Vehicle Emissions. Available online: <https://www.concawe.eu/publication/expectations-actual-euro-6-vehicle-emissions/> (accessed on 27 January 2021).
71. Park, J.; Shin, M.; Lee, J.; Lee, J. Estimating the effectiveness of vehicle emission regulations for reducing NO<sub>x</sub> from light-duty vehicles in Korea using on-road measurements. *Sci. Total Environ.* **2021**, *767*, 144250. [CrossRef]
72. Triantafyllopoulos, G.; Katsaounis, D.; Karamitros, D.; Ntziachristos, L.; Samaras, Z. Experimental assessment of the potential to decrease diesel NO<sub>x</sub> emissions beyond minimum requirements for Euro 6 Real Drive Emissions (RDE) compliance. *Sci. Total Environ.* **2018**, *618*, 1400–1407. [CrossRef]
73. Du, B.; Zhang, L.; Geng, Y.; Zhang, Y.; Xu, H.; Xiang, G. Testing and evaluation of cold-start emissions in a real driving emissions test. *Transp. Res. Part D Transp. Environ.* **2020**, *86*, 102447. [CrossRef]
74. Yang, Z.; Ge, Y.; Thomas, D.; Wang, X.; Su, S.; Li, H.; He, H. Real driving particle number (PN) emissions from China-6 compliant PFI and GDI hybrid electrical vehicles. *Atmos. Environ.* **2019**, *199*, 70–79. [CrossRef]
75. Varella, R.A.; Faria, M.V.; Mendoza-Villafuerte, P.; Baptista, P.C.; Sousa, L.; Duarte, G.O. Assessing the influence of boundary conditions, driving behavior and data analysis methods on real driving CO<sub>2</sub> and NO<sub>x</sub> emissions. *Sci. Total Environ.* **2019**, *658*, 879–894. [CrossRef] [PubMed]
76. Lenz, M.; Hoehl, T.; Zanger, L.; Pischinger, S. Approach to determine the entropy coefficient of a battery by numerical optimization. *J. Power Sources* **2020**, *480*, 228841. [CrossRef]
77. Chindamo, D.; Gadola, M. What is the Most Representative Standard Driving Cycle to Estimate Diesel Emissions of a Light Commercial Vehicle? *IFAC-PapersOnLine* **2018**, *51*, 73–78. [CrossRef]
78. Napolitano, P.; Guido, C.; Beatrice, C.; Pellegrini, L. Impact of hydrocracked diesel fuel and Hydrotreated Vegetable Oil blends on the fuel consumption of automotive diesel engines. *Fuel* **2018**, *222*, 718–732. [CrossRef]
79. Scaradozzi, D.; Fanesi, M. Advanced Control Strategies to Improve Nonlinear Automotive Dynamical Systems Consumption. *Axioms* **2019**, *8*, 123. [CrossRef]
80. Institute of Internal Combustion Engines and Thermodynamics. Measurement of CO<sub>2</sub>- and Fuel Consumption from Cars in the NEDC and in Real-World-Driving Cycles. Available online: <https://ermes-group.eu/web/system/files/filedepot/9/2009-TUG-NEDC-real-world-CO2.pdf> (accessed on 28 January 2021).
81. Association for Emissions Control by Catalyst (AECC). Particulate Emissions from Typical Light-Duty Vehicles Taken from the European Fleet, Equipped with a Variety of Emissions Control Technologies. Available online: [https://www.nanoparticles.ch/archive/2011\\_May\\_PR.pdf](https://www.nanoparticles.ch/archive/2011_May_PR.pdf) (accessed on 28 January 2021).
82. The Mobile Air-Conditioning Systems MACs. Available online: [https://ec.europa.eu/growth/sectors/automotive/environment-protection/mobile-air-conditioning-systems\\_en](https://ec.europa.eu/growth/sectors/automotive/environment-protection/mobile-air-conditioning-systems_en) (accessed on 28 January 2021).
83. Li, C.; Brewer, E.; Pham, L.; Jung, H. Reducing Mobile Air Conditioner (MAC) Power Consumption Using Active Cabin-Air-Recirculation in A Plug-In Hybrid Electric Vehicle (PHEV). *World Electr. Veh. J.* **2018**, *9*, 51. [CrossRef]
84. Shendge, S.; Tilekar, P.; Dahiya, S.; Kapoor, S. *Reduction of MAC Power Requirement in a Small Car*; 2010-01-0803; SAE International: Warrendale, PA, USA, 2010.
85. Monforte, R.; Lovuolo, F.; Rostagno, M.; Seccardini, R. *New MAC Technologies: Fuel Efficiency Effect in Real Driving of the Air Intake Flap Management*; 2015-01-1609; SAE International: Warrendale, PA, USA, 2015.
86. Sciance, F.; Nelson, B.; Yassine, M.; Patti, A.; Rao, L. *Developing the AC17 Efficiency Test for Mobile Air Conditioners*; 2013-01-0569; SAE International: Warrendale, PA, USA, 2013.
87. Kim, J.; Choi, K.; Myung, C.L.; Lee, Y.; Park, S. Comparative investigation of regulated emissions and nano-particle characteristics of light duty vehicles using various fuels for the FTP-75 and the NEDC mode. *Fuel* **2013**, *106*, 335–343. [CrossRef]
88. Zhang, C.; Miller, E.; Kotz, A.; Kelly, K.; Thornton, M.; Geller, M.; Brezny, R. Characterization of commercial vehicles' start-up operations from in-use data. *Transp. Res. Part D Transp. Environ.* **2021**, *91*, 102694. [CrossRef]
89. Myung, C.L.; Jang, W.; Kwon, S.; Ko, J.; Jin, D.; Park, S. Evaluation of the real-time de-NO<sub>x</sub> performance characteristics of a LNT-equipped Euro-6 diesel passenger car with various vehicle emissions certification cycles. *Energy* **2017**, *132*, 356–369. [CrossRef]
90. Myung, C.L.; Choi, K.; Kim, J.; Lim, Y.; Lee, J.; Park, S. Comparative study of regulated and unregulated toxic emissions characteristics from a spark ignition direct injection light-duty vehicle fueled with gasoline and liquid phase LPG (liquefied petroleum gas). *Energy* **2012**, *44*, 189–196. [CrossRef]
91. Roso, V.R.; Santos, N.D.S.A.; Valle, R.M.; Alvarez, C.E.C.; Monsalve-Serrano, J.; García, A. Evaluation of a stratified prechamber ignition concept for vehicular applications in real world and standardized driving cycles. *Appl. Energy* **2019**, *254*, 113691. [CrossRef]
92. Benajes, J.; García, A.; Monsalve-Serrano, J.; Sari, R.L. Fuel consumption and engine-out emissions estimations of a light-duty engine running in dual-mode RCCI/CDC with different fuels and driving cycles. *Energy* **2018**, *157*, 19–30. [CrossRef]

93. Kim, J.; Kim, K.; Oh, S. An assessment of the ultra-lean combustion direct-injection LPG (liquefied petroleum gas) engine for passenger-car applications under the FTP-75 mode. *Fuel Process. Technol.* **2016**, *154*, 219–226. [CrossRef]
94. Jhang, S.R.; Lin, Y.C.; Chen, K.S.; Lin, S.L.; Batterman, S. Evaluation of fuel consumption, pollutant emissions and well-to-wheel GHGs assessment from a vehicle operation fueled with bioethanol, gasoline and hydrogen. *Energy* **2020**, *209*, 118436. [CrossRef]
95. Hu, Z.; Lu, Z.; Song, B.; Quan, Y. Impact of test cycle on mass, number and particle size distribution of particulates emitted from gasoline direct injection vehicles. *Sci. Total Environ.* **2021**, *762*, 143128. [CrossRef] [PubMed]
96. Supplemental Federal Test Procedures; Overview. Available online: [https://www.govregs.com/regulations/expand/title40\\_chapterI-i36\\_part1066\\_subpartI\\_section1066.830](https://www.govregs.com/regulations/expand/title40_chapterI-i36_part1066_subpartI_section1066.830) (accessed on 29 January 2021).
97. Lee, J.S. Stability Analysis of Deadbeat-Direct Torque and Flux Control for Permanent Magnet Synchronous Motor Drives with Respect to Parameter Variations. *Energies* **2018**, *11*, 2027. [CrossRef]
98. Rask, E.; Bocci, D.; Duoba, M.; Lohse-Busch, H. Model Year 2010 Ford Fusion Level-1 Testing Report. Available online: <https://www.osti.gov/biblio/993395-model-year-ford-fusion-level-testing-report> (accessed on 29 January 2021).
99. Continental. Worldwide Emission Standards and Related Regulations. Passenger Cars/Light and Medium Duty Vehicles May 2019. Available online: <https://www.continental-automotive.com/getattachment/8f2dedad-b510-4672-a005-3156f77d1f85/EMISSIONBOOKLET2019.pdf> (accessed on 29 January 2021).
100. Delphi. Worldwide Emission Standards. Passenger Cars and Light Duty. Available online: <https://www.delphi.com/sites/default/files/inline-files/delphi-worldwide-emissions-standards-passenger-cars-light-duty-2016-7.pdf> (accessed on 29 January 2021).
101. EPA Emission Standards for Light-Duty Vehicles and Trucks and Motorcycles. Available online: <https://www.epa.gov/emission-standards-reference-guide/epa-emission-standards-light-duty-vehicles-and-trucks-and> (accessed on 29 January 2021).
102. Khan, T.; Frey, H.C. Comparison of real-world and certification emission rates for light duty gasoline vehicles. *Sci. Total Environ.* **2018**, *622–623*, 790–800. [CrossRef] [PubMed]
103. Saw, L.H.; Poon, H.M.; Chong, W.T.; Wang, C.T.; Yew, M.C.; Yew, M.K.; Ng, T.C. Numerical modeling of hybrid supercapacitor battery energy storage system for electric vehicles. *Energy Procedia* **2019**, *158*, 2750–2755. [CrossRef]
104. Changizian, S.; Ahmadi, P.; Raeesi, M.; Javani, N. Performance optimization of hybrid hydrogen fuel cell-electric vehicles in real driving cycles. *Int. J. Hydrogen Energy* **2020**, *45*, 35180–35197. [CrossRef]
105. Giakoumis, E.G. Light-Duty Vehicles. In *Driving and Engine Cycles*, 1st ed.; Giakoumis, E.G., Ed.; Springer: Cham, Switzerland, 2017; Volume 1, pp. 65–166.
106. Nam, E.K.; Colvin, A.D. *An Experimental Procedure for Simulating an SC03 Emissions Test with Air Conditioner On*; SAE Technical Paper 2004-01-0594; SAE International: Warrendale, PA, USA, 2004.
107. McDonald, J. Progress in the Development of Tier 2 Light-Duty Diesel Vehicles. Available online: <http://www.4cleanair.org/Oldmembers/members/committee/mobile/Progressindev.pdf> (accessed on 29 January 2021).
108. Samuel, S.; Austin, L.; Morrey, D. Automotive test drive cycles for emission measurement and real-world emission levels—A review. *Proc. Inst. Mech. Eng. Part D J. Automob. Eng.* **2002**, *216*, 555–564. [CrossRef]
109. Exhaust Emission Test Procedures for Motor Vehicles. Available online: <https://www.govinfo.gov/content/pkg/CFR-2016-title40-vol37/pdf/CFR-2016-title40-vol37-part1066-subpartI.pdf> (accessed on 29 January 2021).
110. Accounting for the Variation of Driver Aggression in the Simulation of Conventional and Advanced Vehicles. Available online: <https://www.nrel.gov/docs/fy13osti/57503.pdf> (accessed on 7 February 2021).
111. Wasiak, A. *Modeling Energetic Efficiency of Biofuels Production*. *Green Energy and Technology*, 1st ed.; Springer Nature Switzerland: Cham, Switzerland, 2018; pp. 29–47. ISBN 978-3-319-98430-8. [CrossRef]
112. Tucki, K.; Orynych, O.; Swi c, A.; Mitoraj-Wojtanek, M. The Development of Electromobility in Poland and EU States as a Tool for Management of CO<sub>2</sub> Emissions. *Energies* **2019**, *12*, 2942. [CrossRef]
113. Dziku c, M.; Piwowar, A.; Szufa, S.; Adamczyk, J.; Dziku c, M. Potential and Scenarios of Variants of Thermo-Modernization of Single-Family Houses: An Example of the Lubuskie Voivodeship. *Energies* **2021**, *14*, 191. [CrossRef]
114. Saggi, M.H.; Sheikh, N.A.; Muhamad Niazi, U.; Irfan, M.; Glowacz, A.; Legutko, S. Improved Analysis on the Fin Reliability of a Plate Fin Heat Exchanger for Usage in LNG Applications. *Energies* **2020**, *13*, 3624. [CrossRef]
115. Kropiwnicki, J. A unified approach to the analysis of electric energy and fuel consumption of cars in city traffic. *Energy* **2019**, *182*, 1045–1057. [CrossRef]
116. Tucki, K.; Mruk, R.; Orynych, O.; Gola, A. The Effects of Pressure and Temperature on the Process of Auto-Ignition and Combustion of Rape Oil and Its Mixtures. *Sustainability* **2019**, *11*, 3451. [CrossRef]
117. Potter, A.; Graham, S. Supplier involvement in eco-innovation: The co-development of electric, hybrid and fuel cell technologies within the Japanese automotive industry. *J. Clean. Prod.* **2019**, *210*, 1216–1228. [CrossRef]
118. Pichler, M.; Krenmayr, N.; Schneider, E.; Brand, U. EU industrial policy: Between modernization and transformation of the automotive industry. *Environ. Innov. Soc. Transit.* **2021**, *38*, 140–152. [CrossRef]
119. Jiao, J.; Zuo, F.; Li, L.; Yuan, J.; Li, J. Estimation of China’s alternative policies of automotive fuels—A perspective of oil dependence. *J. Clean. Prod.* **2017**, *161*, 698–707. [CrossRef]
120. Lapuerta, M.; Rodr guez-Fern ndez, J.; Garc a-Contreras, R. Effect of a glycerol-derived advanced biofuel—FAGE (fatty acid formal glycerol ester)—on the emissions of a diesel engine tested under the New European Driving Cycle. *Energy* **2015**, *93*, 568–579. [CrossRef]

121. Martins, J.; Brito, F.P. Alternative Fuels for Internal Combustion Engines. *Energies* **2020**, *13*, 4086. [CrossRef]
122. Chłopek, Z.; Zakrzewska, D. The criteria for the assessment energy carriers as replacement fuels for internal combustion engines. *TTS Tech. Transp. Szyn.* **2015**, *22*, 278–283.
123. Krakowski, R. Alternative fuels and drives in the context of tightening emission regulations. *Autobusy Tech. Eksploat. Syst. Transp.* **2017**, *18*, 1225–1230.
124. Baczewski, K.; Kałdoński, T. *Paliwa do Silników o Zapłonie Iskrowym*, 2nd ed.; WKŁ Wydawnictwa Komunikacji i Łączności: Warszawa, Poland, 2008; pp. 40–191.
125. Ballesteros, M.; Manzanares, P. Liquid Biofuels. In *The Role of Bioenergy in the Bioeconomy*, 1st ed.; Lago, C., Caldes, N., Lechón, Y., Eds.; Academic Press: London, UK, 2019; pp. 113–144.
126. Mailaram, S.; Kumar, P.; Kunamalla, A.; Saklecha, P.; Maity, S.K. Biomass, biorefinery, and biofuels. In *Sustainable Fuel Technologies Handbook*, 1st ed.; Dutta, S., Hussain, C.M., Eds.; Academic Press: London, UK, 2021; pp. 51–87.
127. Speight, J.G. *The Refinery of the Future*, 2nd ed.; Gulf Professional Publishing: Oxford, UK; Elsevier: Oxford, UK, 2020; pp. 391–426.
128. Dooley, S.; Won, S.H.; Dryer, F.L. Surrogate fuels and combustion characteristics of liquid transportation fuels. In *Computer Aided Chemical Engineering*, 1st ed.; Faravelli, T., Manenti, F., Ranzi, E., Eds.; Elsevier: Oxford, UK, 2019; pp. 513–602.
129. Martyr, A.J.; Rogers, D.R. *Engine Testing*, 5th ed.; Elsevier: Oxford, UK, 2019; pp. 511–535.
130. Cieśliński, J.; Kaczmarczyk, T.; Dawidowicz, B. Performance of the PEM fuel cell module. Part 2. Effect of excess ratio and stack temperature. *J. Power Technol.* **2017**, *97*, 246–251.
131. Smolarz, A. *Diagnostyka Procesów Spalania Paliw Gazowych, Pyłu Węglowego Oraz Mieszanki Pyłu Węglowego i Biomasy z Wykorzystaniem Metod Optycznych*, 1st ed.; Politechnika Lubelska: Lublin, Poland, 2013; pp. 17–40.
132. Borkowski, J.; Szada-Borzyszkowski, W. The possibilities and consequences of the use of coal-water slurry as an alternative fuel to power diesel engines. *Autobusy Tech. Eksploat. Syst. Transp.* **2014**, *15*, 72–75.
133. Hänggi, S.; Elbert, P.; Büttler, T.; Cabalzar, U.; Teske, S.; Bach, C.; Onder, C. A review of synthetic fuels for passenger vehicles. *Energy Rep.* **2019**, *5*, 555–569. [CrossRef]
134. Shcheklein, S.E.; Dubinin, A.M. Analysis of nitrogen oxide emissions from modern vehicles using hydrogen or other natural and synthetic fuels in combustion chamber. *Int. J. Hydrogen Energy* **2020**, *45*, 1151–1157. [CrossRef]
135. Synthetic Fuels—The Next Revolution? Available online: <https://www.bosch.com/stories/synthetic-fuels/> (accessed on 30 January 2021).
136. Trost, T.; Sterner, M.; Bruckner, T. Impact of electric vehicles and synthetic gaseous fuels on final energy consumption and carbon dioxide emissions in Germany based on long-term vehicle fleet modeling. *Energy* **2017**, *141*, 1215–1225. [CrossRef]
137. Synthetic Fuels Ready for Serial Use in Passenger Cars by 2030—Porsche CEO. Available online: <https://www.cleanenergywire.org/news/synthetic-fuels-ready-serial-use-passenger-cars-2030-porsche-ceo> (accessed on 30 January 2021).
138. Rashid, A.K.; Mansor, M.R.A.; Racovitza, A.; Chiriac, R. Combustion Characteristics of Various Octane Rating Fuels for Automotive Thermal Engines Efficiency Requirements. *Energy Procedia* **2019**, *157*, 763–772. [CrossRef]
139. Kandasamy, S.K.; Selvaraj, A.S.; Rajagopal, T.K.R. Experimental investigations of ethanol blended biodiesel fuel on automotive diesel engine performance, emission and durability characteristics. *Renew. Energy* **2019**, *141*, 411–419. [CrossRef]
140. Tucki, K.; Mruk, R.; Orynych, O.; Wasiak, A.; Świć, A. Thermodynamic Fundamentals for Fuel Production Management. *Sustainability* **2019**, *11*, 4449. [CrossRef]
141. Garrett, T.K.; Newton, K.; Steeds, W. Fuels and their combustion. In *Motor Vehicle*, 13th ed.; Garrett, T.K., Newton, K., Steeds, W., Eds.; Elsevier: Oxford, UK, 2019; pp. 590–618.
142. Pałuchowska, M.; Jakóbiec, J. Effects of ethanol addition and chemical composition of the fuel on its performance parameters. *Autobusy Tech. Eksploat. Syst. Transp.* **2012**, *13*, 140–149.
143. Speight, J.G.; El-Gendy, N.S. Refinery Products and By-Products. In *Introduction to Petroleum Biotechnology*, 1st ed.; Speight, J.G., El-Gendy, N.S., Eds.; Gulf Professional Publishing: Oxford, UK, 2010; pp. 41–68.
144. Coker, A.K. Petroleum, Complex-Mixture Fractionation, Gas Processing, Dehydration, Hydrocarbon Absorption and Stripping; Part 2: Fractionation. In *Ludwig's Applied Process Design for Chemical and Petrochemical Plants*, 4th ed.; Fractionation; Coker, A.K., Ed.; Gulf Professional Publishing: Oxford, UK, 2018; pp. 269–344.
145. Tian, Y.; You, X.; Huang, X. SDAE-BP Based Octane Number Soft Sensor Using Near-infrared Spectroscopy in Gasoline Blending Process. *Symmetry* **2018**, *10*, 770. [CrossRef]
146. Rodríguez-Fernández, J.; Ramos, Á.; Barba, J.; Cárdenas, D.; Delgado, J. Improving Fuel Economy and Engine Performance through Gasoline Fuel Octane Rating. *Energies* **2020**, *13*, 3499. [CrossRef]
147. Klimov, A.V.; Panov, S.B.; Serdiuk, L.A.; Ashkinazi, L.A. Industrial cleaning of fuel by means of porous polymeric materials. *Rocz. Ochr. Środowiska (Annu. Set Environ. Prot.)* **2007**, *9*, 55–66.
148. Sastry, S.; Saha, A.; Ghosh, R. Modeling the Dynamics of Carbon Dioxide over an Educational Institute. In *ICT Analysis and Applications. Lecture Notes in Networks and Systems*, 1st ed.; Fong, S., Dey, N., Joshi, A., Eds.; Springer: Singapore, 2020; Volume 93. [CrossRef]
149. How Much CO<sub>2</sub> Comes from Burning a Liter of Gasoline, i.e., Who Drives a Gasoline Engine, Drives an Electrician Parallely. Available online: <https://elektrowoz.pl/porady/ile-co2-jest-ze-spalenia-litra-benzyny-czyli-kto-jezdzi-spalinowka-ten-jezdzi-rownolegle-elektrykiem/> (accessed on 30 January 2021).
150. Pałuchowska, M.; Jakóbiec, J. The quality specification of E10 engine petrol. *Nafta-Gaz* **2011**, *67*, 825–830.

151. Standard Specification for Automotive Spark-Ignition Engine Fuel. Available online: <https://www.astm.org/Standards/D4814.htm> (accessed on 29 January 2021).
152. Zhang, Q.; Qian, X.; Fu, L.; Yuan, M.; Chen, Y. Shock wave evolution and overpressure hazards in partly premixed gas deflagration of DME/LPG blended multi-clean fuel. *Fuel* **2020**, *268*, 117368. [CrossRef]
153. Muhssen, H.S.; Masuri, S.U.; Sahari, B.B.; Hairuddin, A.A. Design improvement of compressed natural gas (CNG)-Air mixer for diesel dual-fuel engines using computational fluid dynamics. *Energy* **2021**, *216*, 118957. [CrossRef]
154. Suarez-Bertoa, R.; Pechout, M.; Vojtíšek, M.; Astorga, C. Regulated and Non-Regulated Emissions from Euro 6 Diesel, Gasoline and CNG Vehicles under Real-World Driving Conditions. *Atmosphere* **2020**, *11*, 204. [CrossRef]
155. Sweelssen, J.; Blokland, H.; Rajamäki, T.; Boersma, A. Capacitive and Infrared Gas Sensors for the Assessment of the Methane Number of LNG Fuels. *Sensors* **2020**, *20*, 3345. [CrossRef]
156. Mahmood, H.A.; Adam, N.M.; Sahari, B.B.; Masuri, S.U. New Design of a CNG-H<sub>2</sub>-AIR Mixer for Internal Combustion Engines: An Experimental and Numerical Study. *Energies* **2017**, *10*, 1373.
157. LPG as an Ecological Fuel. It's What the Climate Summit Should Be Discussing. Available online: <https://autokult.pl/32628lpg-jako-ekologiczne-paliwo-to-o-nim-powinno-sie-dyskutowac-na-szczycie-klimatycznym> (accessed on 6 February 2021).
158. Development of the Methodology and Estimation of Theexternal Costs of Air Pollution Emitted from Roadtransport at National Level. Available online: [https://stat.gov.pl/download/gfx/portalinformacyjny/pl/defaultstronaopisowa/6150/1/1/raport\\_koszty\\_zewnetrzne\\_emisji\\_zanieczyszczen.pdf](https://stat.gov.pl/download/gfx/portalinformacyjny/pl/defaultstronaopisowa/6150/1/1/raport_koszty_zewnetrzne_emisji_zanieczyszczen.pdf) (accessed on 6 February 2021).
159. EEA. Towards Clean and Smart Mobility. Available online: <https://www.eea.europa.eu/publications/signals-2016/download> (accessed on 6 February 2021).
160. Liu, Z.; Jia, W.; Liang, L.; Duan, Z. Analysis of Pressure Pulsation Influence on Compressed Natural Gas (CNG) Compressor Performance for Ideal and Real Gas Models. *Appl. Sci.* **2019**, *9*, 946. [CrossRef]
161. Time for Methane? Alternative Fuels: CNG and LNG under the Loupe. Available online: <http://www.ekspert-flotowy.pl/artykuly/552/czas-na-metan-paliwa-alternatywne-cng-i-lng-pod-lupa.html> (accessed on 6 February 2021).
162. Biofuels—An Alternative to Growing Prices at Fuel Stations? Available online: <http://laboratoria.net/artukul/12597.html> (accessed on 6 February 2021).
163. Rosiak, E. The Global Market for Vegetable Oils. *Sci. J. Wars. Univ. Life Sci. Probl. World Agric.* **2017**, *17*, 173–181.
164. Tucki, K.; Orynych, O.; Wasiak, A.; Świć, A.; Mruk, R.; Botwińska, K. Estimation of Carbon Dioxide Emissions from a Diesel Engine Powered by Lignocellulose Derived Fuel for Better Management of Fuel Production. *Energies* **2020**, *13*, 561. [CrossRef]
165. Tibaquirá, J.E.; Huertas, J.I.; Ospina, S.; Quirama, L.F.; Niño, J.E. Wpływ korzystania z etanolu i benzyny mieszanki na mechaniczne, energii i środowiska pojazdów używanych. *Energies* **2018**, *11*, 221. [CrossRef]
166. Nazimek, D. Liquid biofuel. *Autobusy Tech. Eksploat. Syst. Transp.* **2012**, *13*, 235–240.
167. Żółty, M.; Stepień, Z. Ethanol fuels for spark ignition engines. *Nafta-Gaz* **2016**, *72*, 761–769.
168. More about: Methanol. Available online: <https://www.methanex.com/about-methanol/methanol-vehicle-fuel> (accessed on 6 February 2021).
169. Methanol as an Alternative Transportation Fuel in the US: Options for Sustainable and/or Energy-Secure Transportation. Available online: [https://afdc.energy.gov/files/pdfs/mit\\_methanol\\_white\\_paper.pdf](https://afdc.energy.gov/files/pdfs/mit_methanol_white_paper.pdf) (accessed on 6 February 2021).
170. García, A.; Monsalve-Serrano, J.; Villalta, D.; Guzmán-Mendoza, M. Methanol and OME<sub>x</sub> as fuel candidates to fulfill the potential EURO VII emissions regulation under dual-mode dual-fuel combustion. *Fuel* **2021**, *287*, 119548. [CrossRef]
171. Bechtold, R.L.; Goodman, M.B.; Timbario, T.A. Use of Methanol as a Transportation Fuel. Available online: <http://methanolfuels.org/wp-content/uploads/2013/05/Bechtold-ATS-Methanol-Use-in-Transportation.pdf> (accessed on 6 February 2021).
172. Panda, K.; Ramesh, A. Diesel injection strategies for reducing emissions and enhancing the performance of a methanol based dual fuel stationary engine. *Fuel* **2021**, *289*, 119809. [CrossRef]
173. Vehicle Energy Consumption Calculation Tool—VECTO. Available online: [https://ec.europa.eu/clima/policies/transport/vehicles/vecto\\_en](https://ec.europa.eu/clima/policies/transport/vehicles/vecto_en) (accessed on 6 February 2021).
174. Georgios, Z.N.; Alessandro, T.; Ignacio, P.R.; Theodoros, G.; Georgios, F. *A Generalized Component Efficiency and Input-Data Generation Model for Creating Fleet-Representative Vehicle Simulation Cases in VECTO*; SAE Technical Paper 2019-01-1280; SAE International: Warrendale, PA, USA, 2019. [CrossRef]
175. Analysis of VECTO Data for Heavy-Duty Vehicles (HDV) CO<sub>2</sub> Emission Targets. Available online: <https://ec.europa.eu/jrc/en/publication/eur-scientific-and-technical-research-reports/analysis-vecto-data-heavy-duty-vehicles-hdv-co2-emission-targets> (accessed on 6 February 2021).
176. Zacharof, N.; Özener, O.; Özkan, M.; Kilicaslan, A.; Fontaras, G. Simulating City-Bus On-Road Operation with VECTO. *Frontiers in Mechanical Engineering* 2019. Available online: <https://www.frontiersin.org/articles/10.3389/fmech.2019.00058/full> (accessed on 6 February 2021). [CrossRef]
177. All about CO<sub>2</sub> Emissions Regulations & VECTO. Available online: <https://www.continental-tires.com/transport/fleetsolutions/co2-regulations-vecto> (accessed on 6 February 2021).
178. Rodríguez, F.; Delgado, O. The Future of VECTO: CO<sub>2</sub> Certification of Advanced Heavy-Duty Vehicles in the European Union. Available online: [https://theicct.org/sites/default/files/publications/Future\\_of\\_VECTO\\_CO2\\_certification\\_20191009.pdf](https://theicct.org/sites/default/files/publications/Future_of_VECTO_CO2_certification_20191009.pdf) (accessed on 6 February 2021).

179. Fontaras, G.; Grigoratos, T.; Savvidis, D.; Anagnostopoulos, K.; Luz, R.; Rexeis, M.; Hausberger, S. An experimental evaluation of the methodology proposed for the monitoring and certification of CO<sub>2</sub> emissions from heavy-duty vehicles in Europe. *Energy* **2016**, *102*, 354–364. [CrossRef]
180. CO2MPAS: Vehicle Simulator Predicting NEDC CO<sub>2</sub> Emissions from WLTP. Available online: <https://co2mpas.io/> (accessed on 6 February 2021).
181. Mogno, C.; Fontaras, G.; Arcidiacono, V.; Komnos, D.; Pavlovic, J.; Ciuffo, B.; Makridis, M.; Valverde, V. The application of the CO2MPAS model for vehicle CO<sub>2</sub> emissions estimation over real traffic conditions. *Transp. Policy* **2020**. [CrossRef]
182. Ciuffo, B.; Fontaras, G. Models and scientific tools for regulatory purposes: The case of CO<sub>2</sub> emissions from light duty vehicles in Europe. *Energy Policy* **2017**, *109*, 76–81. [CrossRef]
183. López-Martínez, J.M.; Jiménez, F.; Páez-Ayuso, F.J.; Flores-Holgado, M.N.; Arenas, A.N.; Arenas-Ramirez, B.; Aparicio-Izquierdo, F. Modelling the fuel consumption and pollutant emissions of the urban bus fleet of the city of Madrid. *Transp. Res. Part D Transp. Environ.* **2017**, *52*, 112–127. [CrossRef]
184. 2018 Toyota Camry LE Vehicle Tier 2 Fuel—Test Data Package. Dated 07-30-20. Ann Arbor, MI: US EPA, National Vehicle and Fuel Emissions Laboratory, National Center for Advanced Technology. Available online: <https://www.epa.gov/vehicle-and-fuel-emissions-testing/benchmarking-advanced-low-emission-light-duty-vehicle-technology> (accessed on 7 February 2021).
185. Moskalik, A.; Stuhldreher, M.; Kargul, J. Benchmarking a 2018 Toyota Camry UB80E Eight-Speed Automatic Transmission. SAE 2020-01-1286. 2020. Available online: <https://www.epa.gov/sites/production/files/2020-05/documents/sae-2020-01-1286-benchmark-2018-toyota-camry-ub80e-eight-speed-auto-trans.pdf> (accessed on 7 February 2021). [CrossRef]
186. Kargul, J.; Stuhldreher, M.; Barba, D.; Schenk, C.; Bohac, S.; McDonald, J.; Dekraker, P. Benchmarking a 2018 Toyota Camry 2.5-Liter Atkinson Cycle Engine with Cooled-EGR. *SAE Int. J. Adv. Curr. Pract. Mobil.* **2019**, *1*, 601–638. Available online: <https://www.ncbi.nlm.nih.gov/pmc/articles/PMC7425626/> (accessed on 7 February 2021).
187. Scilab 6.1.0. Available online: <https://www.scilab.org/> (accessed on 7 February 2021).
188. ATOMS: Neural Network Module. Available online: <http://atoms.scilab.org/toolboxes/neuralnetwork/3.0> (accessed on 7 February 2021).
189. Kordylewski, W. *Spalanie i Paliwa*, 5th ed.; Oficyna Wydawnicza Politechniki Wrocławskiej: Wrocław, Poland, 2008; pp. 10–470. ISBN 978-83-7493-378-0.
190. Dobras, S.; Więclaw-Solny, L.; Chwoła, T.; Krótki, A.; Wilk, A.; Tatarczuk, A. Renewable methanol as a fuel and feedstock in the chemical industry. *Zesz. Nauk. Inst. Gospod. Surowcami Miner. I Energią Pan* **2017**, *98*, 27–37.
191. Gwardiak, H.; Rozycki, K.; Ruszkarska, M.; Tylus, J.; Walisiewicz-Niedbalska, W. Evaluation of fatty acid methyl esters (FAME) obtained from various feedstock. *Rośliny Oleiste-Oilseed Crop.* **2011**, *32*, 137–147.
192. Piątkowski, P.; Bohdal, T. Testing of Ecological Properties of Spark Ignition Engine Fed with LPG Mixture. *Rocz. Ochr. Środowiska (Annu. Set Environ. Prot.)* **2011**, *13*, 607–618.
193. The 2020 EPA Automotive Trends Report: Greenhouse Gas Emissions, Fuel Economy, and Technology since 1975. Available online: <https://www.epa.gov/automotive-trends/download-automotive-trends-report#Full%20Report> (accessed on 7 February 2021).
194. Matlab Gearshift Calculation Tool for UN GTR 15. Available online: <https://unece.org/transport/documents/2021/01/standards/matlab-gearshift-calculation-tool-un-gtr-15> (accessed on 7 February 2021).
195. United Nations Economic Commission for Europe. Gearshift Calculation Tool. Available online: <https://wiki.unece.org/display/trans/Gearshift+calculation+tool> (accessed on 7 February 2021).
196. EPA US06 or Supplemental Federal Test Procedure (SFTP). Available online: <https://www.epa.gov/emission-standards-reference-guide/epa-us06-or-supplemental-federal-test-procedure-sftp> (accessed on 7 February 2021).
197. Staff Report. Public Hearing to Consider Adoption of New Certification Tests and Standards to Control Exhaust Emissions from Aggressive Driving and Air-Conditioner Usage for Passenger Cars, Light-Duty Trucks, and Medium-Duty Vehicles under 8501 Pounds Gross Vehicle Weight Rating. Available online: <https://ww3.arb.ca.gov/regact/offcycle/staffrep.pdf> (accessed on 7 February 2021).
198. Eckert, J.J.; Santiciolli, F.M.; Silva, L.C.A.; Dedini, F.G. Vehicle drivetrain design multi-objective optimization. *Mech. Mach. Theory* **2021**, *156*, 104123. [CrossRef]
199. Schenk, C.; Dekraker, P. Potential Fuel Economy Improvements from the Implementation of cEGR and CDA on an Atkinson Cycle Engine. SAE Technical Paper, 2017-01-1016. 2017. Available online: <https://www.epa.gov/sites/production/files/2017-06/documents/sae-2017-01-1016-potential-fuel-economy-improvements-cegr-and-cda-on-atkinson-engine.pdf> (accessed on 7 February 2021). [CrossRef]
200. US: Light-Duty: Highway Fuel Economy Cycle (HWFET). Available online: <https://www.transportpolicy.net/standard/us-light-duty-highway-fuel-economy-cycle-hwfet/> (accessed on 7 February 2021).
201. Choi, Y.; Lee, J.; Jang, J.; Park, S. Effects of fuel-injection systems on particle emission characteristics of gasoline vehicles. *Atmos. Environ.* **2019**, *217*, 116941. [CrossRef]
202. Cho, J.; Kim, K.; Baek, S.; Myung, C.L.; Park, S. Abatement potential analysis on CO<sub>2</sub> and size-resolved particle emissions from a downsized LPG direct injection engine for passenger car. *Atmos. Pollut. Res.* **2019**, *10*, 1711–1722. [CrossRef]
203. EPA Federal Test Procedure (FTP). Available online: <https://www.epa.gov/emission-standards-reference-guide/epa-federal-test-procedure-ftp> (accessed on 7 February 2021).



204. Shen, K.; Chang, I.; Chen, H.; Zhang, Z.; Wang, B.; Wang, Y. Experimental study on the effects of exhaust heat recovery system (EHRS) on vehicle fuel economy and emissions under cold start new European driving cycle (NEDC). *Energy Convers. Manag.* **2019**, *197*, 111893. [CrossRef]
205. Chłopek, Z.; Biedrzycki, J.; Lasocki, J.; Wójcik, P. Pollutant emissions from combustion engine of motor vehicle tested in driving cycles simulating real-world driving conditions. *Zesz. Nauk. Inst. Pojazdów/Politech. Warsz.* **2013**, *1*, 67–76.
206. Bielaczyc, P.; Szczotka, A.; Pajdowski, P.; Woodburn, J. The potential of current European light duty LPG-fuelled vehicles to meet Euro 6 requirements. *Combust. Engines* **2015**, *54*, 874–880.
207. Bielaczyc, P.; Klimkiewicz, D.; Woodburn, J.; Szczotka, A. Exhaust emission testing methods—BOSMAL’s legislative and development emission testing laboratories. *Combust. Engines* **2019**, *58*, 88–98.
208. Exhaust Emission Test Procedure for SC03 Emissions. Available online: <https://www.law.cornell.edu/cfr/text/40/86.160-00> (accessed on 7 February 2021).
209. Random Cycle Generator. Available online: <https://www.tno.nl/en/focus-areas/traffic-transport/roadmaps/sustainable-traffic-and-transport/sustainable-mobility-and-logistics/improving-air-quality-by-monitoring-real-world-emissions/random-cycle-generator/> (accessed on 7 February 2021).
210. Kooijman, D.G.; Balau, A.E.; Wilkins, S.; Ligterink, N.; Cuelenaere, R. WLTP Random Cycle Generator. In Proceedings of the 12th IEEE Vehicle Power and Propulsion Conference (VPPC 2015), Montreal, QC, Canada, 19–22 October 2015; ISBN 9781467376372.
211. Steven, H. WLTP EU Database Short Trip Analysis for Random Cycle Development. Available online: <https://slideplayer.com/slide/17760268/> (accessed on 7 February 2021).
212. Andersson, J.; May, J.; Favre, C.; Bosteels, D.; De Vries, S.; Heaney, M.; Keenan, M.; Mansell, J. On-Road and Chassis Dynamometer Evaluations of Emissions from Two Euro 6 Diesel Vehicles. *SAE* **2014**, *7*, 919–934. [CrossRef]
213. Mobile Air Conditioning (MAC). Test Procedure Development. Available online: <https://unece.org/fileadmin/DAM/trans/doc/2010/wp29grpe/MACTP-01-03e.pdf> (accessed on 7 February 2021).
214. Transitioning to Low-GWP Alternatives in Motor Vehicle Air Conditioning. Available online: [https://www.epa.gov/sites/production/files/2016-12/documents/international\\_transitioning\\_to\\_low-gwp\\_alternatives\\_in\\_mvacs.pdf](https://www.epa.gov/sites/production/files/2016-12/documents/international_transitioning_to_low-gwp_alternatives_in_mvacs.pdf) (accessed on 7 February 2021).
215. Demuyneck, J.; Bosteels, D.; Paeppe, M.D.; Favre, C.; May, J.; Verhelst, S. Recommendations for the new WLTP cycle based on an analysis of vehicle emission measurements on NEDC and CADC. *Energy Policy* **2012**, *49*, 234–242. [CrossRef]
216. Common Artemis Driving Cycles (CADC). Available online: <https://dieselnet.com/standards/cycles/artemis.php> (accessed on 7 February 2021).
217. May, J.; Bosteels, D.; Favre, C. An Assessment of Emissions from Light-Duty Vehicles using PEMS and Chassis Dynamometer Testing. *SAE Int. J. Engines* **2014**, *7*, 1326–1335. [CrossRef]
218. Addendum15: Global Technical Regulation No. 15. Worldwide Harmonized Light Vehicles Test Procedure. Available online: <https://unece.org/fileadmin/DAM/trans/main/wp29/wp29-1998agr-rules/ECE-TRANS-180a15e.pdf> (accessed on 7 February 2021).
219. Ko, J.; Jin, D.; Jang, W.; Myung, C.L.; Kwon, S.; Park, S. Comparative investigation of NO<sub>x</sub> emission characteristics from a Euro 6-compliant diesel passenger car over the NEDC and WLTC at various ambient temperatures. *Appl. Energy* **2017**, *187*, 652–662. [CrossRef]
220. Giechaskiel, B.; Suarez-Bertoa, R.; Lähde, T.; Clairotte, M.; Carriero, M.; Bonnel, P.; Maggiore, M. Evaluation of NO<sub>x</sub> emissions of a retrofitted Euro 5 passenger car for the Horizon prize “Engine retrofit”. *Environ. Res.* **2018**, *166*, 298–309. [CrossRef]
221. Suarez-Bertoa, R.; Zardini, A.A.; Lilova, V.; Meyer, D.; Nakatani, S.; Hibel, F.; Ewers, J.; Clairotte, M.; Hill, L.; Astorga, C. Intercomparison of real-time tailpipe ammonia measurements from vehicles tested over the new world-harmonized light-duty vehicle test cycle (WLTC). *Environ. Sci. Pollut. Res.* **2015**, *22*, 7450–7460. [CrossRef] [PubMed]
222. OPENMODELICA. Available online: <https://openmodelica.org/> (accessed on 7 February 2021).